FATE OF GRAVITATIONAL COLLAPSE IN ELECTROMAGNETIC THEORY

By

Ghulam Abbas

A THESIS
SUBMITTED IN PARTIAL FULFILLMENT OF THE
REQUIREMENTS FOR THE DEGREE OF
DOCTOR OF PHILOSOPHY
IN
MATHEMATICS

Supervised By

Prof. Dr. Muhammad Sharif

UNIVERSITY OF THE PUNJAB
LAHORE-PAKISTAN
SEPTEMBER, 2012

CERTIFICATE

I certify that the research work presented in this thesis is the original work of **Mr. Ghulam Abbas** S/O **Ghulam Muhammad** and is carried out under my supervision. I endorse its evaluation for the award of **Ph.D.** degree through the official procedure of **University of the Punjab**.

Prof. Dr. Muhammad Sharif
(**Supervisor**)

DECLARATION

I, **Mr. Ghulam Abbas** S/O **Ghulam Muhammad**, hereby declare that the matter printed in this thesis is my original work. This thesis does not contain any material that has been submitted for the award of any other degree in any university and to the best of my knowledge, neither does this thesis contain any material published or written previously by any other person, except due reference is made in the text of this thesis.

Ghulam Abbas

DEDICATED

To

My Father (Late) and Mother

Table of Contents

List of Figures

Abstract

In this thesis, we address the issue of gravitational collapse in electromagnetic theory. For this purpose, we adopt two approaches one by assuming charged perfect fluid in the interior of a star and another by studying the dynamics of thin shell of matter on the surface of a charged star. The cylindrically symmetric charged perfect fluid collapse is explored by assuming that charged perfect fluid is moving along geodesics in the interior of cylinder. In this case, the analytic solution of the Einstein-Maxwell field equations represents gravitational collapse. The end state of collapse is found to be conical singularity.

We formulate general dynamical equations using Israel thin shell formalism in charged background which helps to investigate gravitational collapse of scalar field and polytropic matter thin shell. In massless case, we find that scalar shell either expands to infinity or collapses to a point forming a curvature singularity. Also, the massive scalar field shell can exhibit the bouncing behavior. It is found that expanding and collapsing polytropic matter as well as perfect fluid shell comes to rest, then re-expands to infinity or re-collapses to a point. We also discuss the polytropic matter collapse in non-commutative geometry. The non-commutative parameter stops the shell to expand or collapse again, so there occurs a singularity at non-zero value of shell radius.

The charged perfect fluid collapse with positive cosmological constant is investigated in Friedmann and 5D Tolman-Bondi models. We find marginally bound solution for both models and non-marginally bound solution for 5D model. Also, the formation of apparent horizons is discussed. The

end state of charged perfect fluid gravitational collapse in both models has been found as a black hole.

Finally, we discuss phantom energy accretion onto a 5D charged black hole. It is found that if the charge of black hole is larger than its mass, then a black hole is converted into naked singularity. The critical accretion points are investigated. We conclude that when phantom energy accretes onto 5D charged black hole then there appears a mass to charge ratio, the lower limit of this ratio represents a regular as well as extremal 5D charged black holes, while upper limit represents a naked singularity.

Acknowledgements

All praises and thanks to **Allah**, the most beneficent, the most merciful **Who** is the creator of the universe, the Lord of all creatures and have power over all creatures. **Allah** gave me knowledge, intelligence, patience and strength to complete this thesis in time and helped me at each step of my life. Salam from the core of my heart to **The Holy Prophet Muhammad (PBUH) Who** is forever a source of complete guidance and knowledge for Muslim Ummah.

Before any body else, I would like to express my sincere gratitude to my intellectual and competent supervisor, **Prof. Dr. Muhammad Sharif**, for his skillful guidance, never ending support, encouragement and proper check and balance during my research work. I feel proud for the completion of research work under his supervision.

I feel pleasure to thank **Prof. Dr. Shahid S. Siddiqi**, Chairman Department of Mathematics, for providing the research facilities during my research work. I am thankful to all faculty members for their cooperative behavior. A discussion about cylindrical gravitational collapse with **Prof. Dr. Asghar Qadir** at NCP, Islamabad, during a conference is highly acknowledged. It is also my gratitude to thank **Prof. Dr. Jin Lin Han**, for his warm hospitality at National Astronomical Observatories of China (NAOC), Chinese Academy of Sciences Beijing, China, during my three months visit, where introduction and first chapter of thesis were written. Also, many thanks to Mr. Zubair, for his gossips at NAOC. This was really a memorable study tour.

It is my pleasure to thank my friends Dr. Muhammad Jamil Amir, Khalil Ahmad Malik, Tariq Mahmood, Syed Majid Aziz Shah, Syed Muhammad Munawar Shah, Zulfiqar Ali, Ishfaq Ahmad and Muhammad Sohail

Gillani for their moral support and encouragement throughout this period. I especially thank to my school and college teachers Mr. Sultan Mahmood Malik and Mr. Rashid Mahmood Bodla for their best wishes throughout my educational career. I would like to thank my M.Phil and Ph.D research fellows especially to Miss Wajiha Javed, Dr. Rizwana Kausar, Mr. Abdul Jawad, Mr. Hamood Ur Rehman, Mr. Muhammad Azam, Mr. Zeeshan and Mr. Zaeem for their good company during the whole period.

I am really indebted to my family especially, my parents for their sacrifices, love and prayers throughout my life. Many thanks to my father who passed away during my research work, may his soul be in rest and peace. I would like to express my heartiest gratitude to my mother for wishing every success in my life, may she live long. Thanks to my elder brothers Ghulam Qadir and Ghulam Haider for keeping me free from family responsibilities. The prayers and love of my younger brothers and sisters during research work are highly acknowledged. This acknowledgement would remain incomplete if I do not acknowledge my wife Shazia Abbas. She helped me in every way to concentrate on my studies. She was seriously ignored during my research work, many thanks to her for patience and cooperation. Many thanks and regards to my sweet daughter Kinza Abbas, who was ignored during the write up of this thesis.

Finally, I would like to thank Higher Education Commission, Islamabad, Pakistan for its financial support through the *Indigenous Ph.D. 5000 Fellowship Program Batch-IV* during this period.

Lahore **Ghulam Abbas**

September, 2012

Notations

In this thesis, we shall use the signature of the spacetime as $(+,-,-,-)$. All the Greek indices will vary from 0 to 3, if different it will be mentioned and relativistic units will be used in which $G = c = 1$. Also, we shall use the following list of notations and abbreviations.

GR:	General Relativity
BH:	Black Hole
NS:	Naked Singularity
NC:	Non-Commutative
TB:	Tolman-Bondi
RN:	Reissner-Nordström
CCH:	Cosmic Censorship Hypothesis
EoS:	Equation of State
DE:	Dark Energy
Λ:	Cosmological Constant

Introduction

According to the predictions of modern physics, gravity is the weakest force among four fundamental forces. It plays a vital role for studying the large-scale structures due to its long-range nature as compared to other forces. It helps to study the structure formation of galaxies, BHs and inflation of the universe. General Relativity is the best theory for the description of gravitational force in terms of geometry of manifold and its matter contents. It also explains many astrophysical phenomena such as stellar evolution, gravitational collapse and big bang.

Gravitational collapse is defined as the astronomical phenomenon in which a star with mass much larger than the solar mass contracts to a point under the effect of its own gravity. It occurs when internal nuclear fuel of a massive star fails to supply high pressure to balance gravity. According to GR, gravitational collapse of massive objects (having mass $= 10^6 M_\odot - 10^8 M_\odot$, where $M_\odot$ is the mass of the Sun) results to the formation of spacetime singularities in our universe [1]. One of the most debatable problems in GR is the end state of massive star, which undergoes to gravitational collapse after exhausting its nuclear fuel. What would be the nature of singularity forming due to the gravitational collapse? To answer this question, Penrose [2] proposed a hypothesis known as *Cosmic Censorship Hypothesis*, which states that the end state of gravitational collapse must

be a BH under some realistic conditions.

Despite of various attempts over the past four decades, this problem remained unsolved at the foundation of BH physics. By the failure of numerous attempts to establish the CCH, it seems natural to ask what is really the nature of spacetime singularity? This leads to study the dynamics of gravitational collapse in more extensive way in the framework of GR. It is urged that the final fate of the gravitational collapse would be BH or NS depending upon the nature of initial data of the collapse. The existence of NS in gravitational collapse would be predicted if there are some families of timelike geodesics which end at singularity in the past. On the other hand, no such families of geodesics originate from the singularity when end state of the gravitational collapse is BH [3]. In this case, the spacetime singularity would be hidden by the event horizon of gravity, while for NS there is a causal correspondence between the region of spacetime singularity and external observers.

Recently, Virbhadra et al. [4] investigated that nature of singularity in relativistic gravitational collapse can be determined by taking into account the concept of gravitational lensing. Virbhadra and Ellis [5] studied Schwarzschild BH lensing and found that the relativistic images from BH can confirm Schwarzschild spacetime in the vicinity of event horizon. The same authors [6] observed the lensing phenomenon by a NS and conjectured that a weak NS is covered by at least one photon sphere [7], while strong NS cannot be covered by any photon sphere.

Claudel et al. [8] examined the existence of photon sphere in several astrophysical objects. On the basis of this fact, they remarked that if energy conditions are valid for a BH geometry then such a BH is always covered by

at least one photon sphere. Virbhadra and Keeton [9] estimated the time delay in gravitational lensing by a BH as well as NS and predicted that weak CCH can be verified in the framework of GR. Also, Virbhadra [10] pointed out that NS originating in spherically symmetric null dust Vaidya collapse may validate the Seifert's conjecture [11]. The same author [12] presented an improved version of CCH on the basis of gravitational lensing phenomenon.

The study of gravitational collapse in GR started from the pioneer work of Oppenheimer and Snyder [13]. They investigated that spherically symmetric homogenous dust collapse leads to the formation of BH. Initially, it was urged that homogeneity and spherical symmetry of the collapsing model are responsible for the formation of BH. However, Lamitre-Tolman-Bondi solutions [14]-[16] with inhomogeneous dust implied that collapse of such matter would end as shell crossing and shell focusing singularities. Later on, many authors [17]-[19] proved that shell crossing singularity is naked, while shell focusing singularity might represent BH, depending on the choice of initial data of collapse. Hence, it was concluded that homogeneity of the collapsing model is not a sufficient condition for the formation of BH.

In order to generalize the collapsing mater, it becomes necessary to study the collapse of matter with non-vanishing pressure. Misner and Sharp [20] studied perfect fluid collapse and found BH as the end state of gravitational collapse. Vaidya [21] and Santos [22] studied null dust collapse by taking the collapsing model as a radiating star. Ori and Piran [23]-[25] investigated the self-similar spherically symmetric perfect fluid collapse by assuming an EoS $p = k\rho$. They converted the field equations into ordinary differential equations which were solved numerically by including radial null geodesic

equations. They showed that there are solutions which represent NS as well as BH for $0 < k \leqslant 0.4$. This problem was treated analytically by Joshi and Dwivedi [26] and found that there exist only NS solutions in this case.

Cosmological constant (Λ) is the form of DE with EoS parameter, $\omega = -1$ [27]. Its presence in the field equations may alter the generic properties of spacetime. There has been a renowned interest to study the gravitational collapse with non-vanishing cosmological constant. Markovic and Shapiro [28] investigated homogenous dust collapse with positive cosmological constant. Khan and Qadir [29] discussed the singularity free model of gravitational collapse with positive and negative cosmological constant. Lake [30] studied spherically symmetric dust collapse with positive and negative cosmological constant.

Ghosh and Deshkar [31] explored the inhomogeneous higher dimensional spherically symmetric dust collapse with cosmological constant and found BH as end state. Sharif and Ahmad [32] discussed apparent horizons and their physical significance for perfect fluid spherical collapse with positive cosmological constant. They found that positive cosmological constant slows down the rate of gravitational collapse. Debnath et al. [33] studied thermodynamical behavior of collapsing non-adiabatic fluid in the presence of positive cosmological constant. They remarked that thermodynamical relations are independent of cosmological constant.

The current observational evidences of gravitational waves through advance detectors such as LIGO [34], VIRGO [35] and GEO [36] have increased the interest to study the gravitational collapse in cylindrically symmetric systems. The spherical systems are simple and do not provide non-trivial examples of NS in the generic gravitational collapse. Therefore, the study of

the NS formation in cylindrical collapse is much important as compared to spherical systems. Some numerical studies [37]-[39] provide the generation of gravitational waves from cylindrical collapse. These results have been extended analytically by Nakao and Morisawa [40] to study gravitational waves from cylindrical gravitational collapse.

There are also some developments [41]-[47] related to cylindrical collapse, which has improved our understanding about its dynamics. Nolan [48] examined that cylindrical null dust collapse leads to NS. Nakao and Morisawa [49] investigated the gravitational collapse of a cylindrical perfect fluid thick shell. Sharif and Ahmad [50] extended this work for two perfect fluid cylindrical collapse and discussed the generation of gravitational waves. Di Prisco et al. [51] studied the shearfree gravitational collapse of the anisotropic fluid in the cylindrically symmetric spacetime.

Israel [52] introduced thin shell formalism to obtain the exact solution of dynamical systems in GR. The same author [53] also studied dynamics of dust shell in vacuum. This formalism was extended to charged thin shell by De La Cruz and Israel [54]. Later on, the gravitational instability and collapse of charged perfect fluid thin shell were explored by Kuchar [55] and Chase [56]. Boulware [57] examined the dynamical behavior of charged thin shell and showed that a physical matter collapse may not end as NS. The dynamics of thin matter shell with polytropic EoS was studied by Kijowski and Magli [58]. Pereira and Wang [59] examined cylindrical matter shell composed of dust by using thin shell formalism. Sharif and his collaborators [60]-[62] discussed the dynamics of collapsing perfect fluid thin shell.

Kaluza and Klein [63]-[66] introduced the idea of extension of four dimensions to five dimensions (5D) for the unification of gravitation and electromagnetism. The 5D solutions are much interesting in GR because 10D and 11D solutions in higher dimensional theories of gravity recover 5D solutions by reducing dimensions [67]. The nature of spacetime singularity in 5D is one of the well motivated problems in GR. Ilah and Lemos [68] extended the Oppenheimer and Snyder collapse model to higher dimensions. Sil and Chatterjee [69] proved that for 5D inhomogeneous TB collapsing model, there exist a minimum critical value of inhomogeneity parameter for which solutions represent BH.

Ghosh and Saraykar [70] investigated gravitational collapse in 5D Vaidya geometry and found curvature singularity. Ghosh et al. [71] studied 5D dust collapse in TB spacetime with positive cosmological constant. Sharif and Ahmad [72, 73] generalized this for perfect fluid with positive cosmological constant. Jhingan and Ghosh [74] studied dust collapse in 5D Einstein-Gauss-Bonnet gravity. They found counter examples to CCH and hoop conjecture. Maeda [75] examined the effects of Gauss-Bonnet term on the nature of spacetime singularity in 5D dust collapse. Banerjee et al. [76] showed that for 5D marginally bound collapse, there appears NS which might be covered by increasing the dimensions of the spacetime.

Wheeler and his collaborator [77, 78] investigated the scalar field in GR. Although, there are no observational evidences about the existence of such fields, but theoretically scalar field models are much important in inflationary universe models. It has been found that when such a model collapses, the end state is the primordial BH [79]. In this regard, the study of massive scalar field collapse is strongly motivated in GR. Kaup [80] formulated the

first complex massive scalar field model. Ruffini and Bonazzola [81] discussed the equilibrium conditions for boson stars (compact objects that are composed of scalar fields) models. Recently, a lot of work has been done to investigate the nature of spacetime singularity for massless scalar field [82]-[88].

Goncalves [89] examined the dynamics of collapsing massive scalar field in Einstein de-Sitter background. Chambers et al. [90] discussed the critical behavior of the scalar field during spherically symmetric gravitational collapse. Virbhadra et al. [91] found that there exists a class of static scalar field solutions which satisfies the energy conditions and represent NS. Goswami and Joshi [92] derived a class of scalar field solutions which lead to violation of CCH. Bhatachraya et al. [93] formulated some conditions under which a collapsing scalar field undergoes to sudden dispersal. Núñez et al. [94] discussed the dynamics of massless and massive scalar field thin shell in Schwarzschild geometry.

In classical GR, the curvature singularity is such a point where physical description of the gravitational field is impossible. This problem can be removed in GR by taking into account the quantum mechanical treatment to the standard formulation of GR. Motivated by such reasoning, some BH solutions in NC field theory have been derived. In these solutions, curvature singularity at origin is removed by de-Sitter core which is introduced due to NC nature of spacetime [95]. Nicolini and his collaborators [96]-[98] developed NC version of all the well-known BHs (i.e., Schwarzschild, RN, Kerr and Kerr-Newmann BHs) and discussed their thermodynamical behavior. Bastos et al. [99, 100] explored the singularity problem and discussed some NC BHs. Recently, Bartolami and Zarro [101] have investigated that NC

factor affects the matter dispersion relation and EoS. Motivated by such NC correction to BHs, Oh and Park [102] formulated the thin shell collapse model in NC Schwarzschild geometry. They investigated the effects of NC parameter on the singularity formation.

It is well-known that when phantom energy from an external source accretes onto BH, then mass of BH decreases such that it eventually attains extremal state and finally converts to NS. During accretion process, charge and angular momentum remain unchanged. In Newtonian theory, the problem of accretion of matter onto the compact object was formulated by Bondi [103]. Michel [104] derived the relativistic formula for the accretion of perfect fluid onto the Schwarzschild BH. Sun [105] discussed phantom energy accretion onto BH in the cyclic universe.

Babichev et al. [106] investigated that phantom accretion onto a BH can decrease its mass if the back reaction effects of accreting phantom fluid on geometry of BH are neglected. Jamil et al. [107] discussed the critical accretion on the RN BH. They determined a mass to charge ratio beyond which a BH can be converted into a NS. The same conclusion was drawn by Babichev et al. [108], by using the linear EoS and Chaplygin gas EoS for RN BH. Madrid and Gonzalez [109] showed that accreting phantom energy onto Kerr BH can convert it into a NS. Sharif and Abbas [110]-[112] discussed the phantom energy accretion onto a class of BHs and found that CCH is valid for phantom accretion onto a stringy charged BH.

The implementation of electromagnetic field in cosmological and astrophysical processes is an attractive research area in theoretical physics. Many investigations in this direction are devoted to understand the interaction between electromagnetic and gravitational fields. However, little is

known about the effects of electromagnetic field on gravitational collapse of massive objects. Thorne [113, 114] studied cylindrically symmetric gravitational with magnetic field and concluded that magnetic field can prevent the collapse of cylinder before singularity formation. Ardvan and Partovi [115] investigated dust solution of the field equations with electromagnetic field and found that the electrostatic force is balanced by gravitational force during collapse of charged dust.

Stein-Schabes [116] investigated that charged matter collapse may produce NS instead of BH. Germani and Tsagas [117] discussed the collapse of magnetized dust in TB model. Kouretsis and Tsagas [118] explored the aspects of charged collapse and concluded that electromagnetic tension acts against the gravitational collapse. Further, Tsagas and his collaborators [119]-[130] have implemented electromagnetic field in many cosmological and astrophysical scenarios. Recently, Herrera and his collaborators [131, 132] have discussed the role of electromagnetic field on structure scalars and dynamics of self-gravitating objects. Sharif and Bhatti [133, 134] have extended this work for cylindrical and plane symmetries.

In this thesis, we explore the issue of spherical and cylindrical gravitational collapse in the context of electromagnetic theory. For this purpose, we solve the Einstein-Maxwell field equations with perfect fluid in spherical and cylindrical geometrises and use the Israel thin shell formalism in spherical charged background. Moreover, we investigate the status of CCH through the phantom energy accretion onto 5D charged BH. The thesis is organized as follows:

- In chapter **One**, we briefly discuss basic concepts of electromagnetic theory and gravitational collapse.

- Chapter **Two** deals with the cylindrically symmetric charged perfect fluid gravitational collapse. For the analytic solution of the field equations, we assume that the charged fluid is moving along the geodesics (with constant velocity). The physical properties of solution represent gravitational collapse. Further, we match the interior charged non-static solution to exterior charged static solution, leading to the relationship between the quantities in two regions of the collapsing cylindrical star.

- Chapter **Three** is devoted to discuss the thin shell collapse of scalar field and polytropic matter in the charged background using the Israel thin shell formalism. In this case, numerical solutions are presented to discuss the motion of thin shell. Further, the effects of NC parameter on the collapsing polytropic shell are investigated in detail. We find that massless and massive scalar field thin shells exhibit expanding, collapsing and oscillating behavior. In case of polytropic matter, thin shell collapses to zero size and NC prevents the singularity formation at zero radius.

- In chapter **Four**, we discuss spherically symmetric charged perfect fluid collapse in Friedmann universe model and generalized 5D model. Using junction conditions, the solution of the Einstein-Maxwell equations is found with positive cosmological constant. The effects of electromagnetic field on time formation of the horizons are explored. In both models, we find BH as the end state of gravitational collapse.

- Phantom energy accretion onto 5D charged BH is presented in chapter **Five**. In this case, we find that mass of BH decreases. Further, mass

to charge ratio, critical accretion points and status of CCH have been analyzed in detail.

- We conclude our results in chapter **Six** and also outline some future research directions.

Chapter 1

Electromagnetic Theory and Gravitational Collapse

This chapter contains a brief review of the basic concepts related to electromagnetic theory and gravitational collapse.

1.1 Charged Compact Stars in General Relativity

On the basis of Eddington theory [135] of gaseous stars, Rosseland [136] investigated that a star might contain equal number of positive ions and electrons. A large number of electrons (as compared to positive ions) due to their higher kinetic energy run to escape from its surface. In this way, a star would contain only positive ions. This escape of electrons from the surface of star will continue until the electric field induced inside the star prevents more electrons to escape from its surface. Later on, it was proved that during this process, a star would attain electric charge approximately 100 Coulombs per solar mass [137]. However, for very dense objects, high density and relativistic effects must be taken into account.

A star can experience relativistic effects in strong gravitational field and

require more charge to attain the equilibrium position. For a dense compact star (having mass greater than the solar mass), electric field will be more stronger than the Sun. For example, for equal amount of charge on the surfaces of the Sun and neutron star, electric field on the surface of neutron star would be 10^9 times stronger than on the surface of the Sun [138]. Thus a small amount of charge on the compact stars would produce strong electromagnetic field, which affects geometry of the star significantly. On the basis of this fact, gravitational collapse of charged stars in GR deserve more investigations.

1.2 The Maxwell Equations

The energy-momentum tensor for electromagnetic field is given [139] as

$$T^{(em)}_{\mu\nu} = \frac{1}{4\pi}(-g^{\delta\omega}F_{\mu\delta}F_{\nu\omega} + \frac{1}{4}g_{\mu\nu}F_{\delta\omega}F^{\delta\omega}), \tag{1.2.1}$$

where $F_{\mu\nu}$ is the Maxwell field tensor defined as

$$F_{\mu\nu} = \phi_{\nu,\mu} - \phi_{\mu,\nu} \tag{1.2.2}$$

and ϕ_μ is the four potential. The time component of the four potential gives electric scalar potential and spatial components yield magnetic vector potential. The electromagnetic energy-momentum tensor in mixed form is

$$T^{(em)\mu}_{\ \ \nu} = \frac{1}{4\pi}(-F^{\mu\omega}F_{\nu\omega} + \frac{1}{4}\delta^\mu_\nu F_{\delta\omega}F^{\delta\omega}). \tag{1.2.3}$$

Its trace is $T^{(em)} = 0$ only in four-dimensional case, otherwise it will be non-zero. This energy-momentum tensor does not obey conservation law [140] as

$$T^{(em)\mu\nu}_{\ \ \ ;\nu} = -F^{\mu\nu}J_\nu, \tag{1.2.4}$$

where J_ν is the four current.

The components of the energy-momentum tensor can be obtained by solving the Maxwell equations for background spacetime. In classical electromagnetic theory, there are four fundamental equations known as Maxwell equations. We can write their differential form as follows [141]

$$\nabla.\mathbf{E} = \frac{\rho_e}{\epsilon_0}, \tag{1.2.5}$$

$$\nabla.\mathbf{B} = 0, \tag{1.2.6}$$

$$\nabla\times\mathbf{E} = -\frac{\partial\mathbf{B}}{\partial t}, \tag{1.2.7}$$

$$\nabla\times\mathbf{B} = \mu_0\mathbf{J} + \frac{1}{c^2}\frac{\partial\mathbf{E}}{\partial t}. \tag{1.2.8}$$

The quantities $\mathbf{E},\ \mathbf{B},\ \rho_e,\ \mathbf{J},\ \epsilon_0$ and μ_0 represent electric field, magnetic field, charge density, current density, permittivity and permeability respectively. Moreover, magnetic field $\mathbf{B}$ and magnetic field intensity $\mathbf{H}$ are related by $\mathbf{B} = \mu_0\mathbf{H}$. A comprehensive description of the Maxwell equations is as follows:

- Equation (1.2.5) describes Gauss law of electricity which shows how electric field diverges from electric charge.
- Equation (1.2.6) is a Gauss law of magnetism which states that there are no isolated magnetic poles.
- Equation (1.2.7) gives Faraday law which describes that electric field is produced by changing magnetic field.
- Ampere law (1.2.8) states that changing electric fields and electric currents produce the circulating magnetic fields.

In tensor formalism, the Maxwell equations can be written in the following form [139]

$$F^{\mu\nu}_{;\nu} = 4\pi J^{\mu}, \quad F_{[\mu\nu;\lambda]} = 0. \tag{1.2.9}$$

1.3 Einstein-Maxwell Field Equations

The Einstein-Maxwell field equations for a charged gravitating system are

$$G_{\mu\nu} = 8\pi(T^{(m)}_{\mu\nu} + T_{\mu\nu}{}^{(em)}), \tag{1.3.1}$$

where $G_{\mu\nu}$ is the Einstein tensor, $T^{(m)}_{\mu\nu}$ is the matter energy-momentum tensor and $T_{\mu\nu}{}^{(em)}$ is the electromagnetic energy-momentum tensor. Since the derivation of the Einstein-Maxwell field equations, relativists have been suggesting several models of charged gravitating objects by considering different matter sources along with electromagnetic field. These models can explain the physical nature of massive objects like neutron star, BH, pulsar, quark star and quasar. These dense objects can be classified in terms of their masses as white dwarf (mass $< 1.44M_{\odot}$), quark star ($2M_{\odot} - 3M_{\odot}$) and neutron star ($1.35M_{\odot} - 2.1M_{\odot}$) [142].

The classical solution of the Einstein-Maxwell field equations is the RN solution, which describes exterior gravitational field of massive charged object. It has two singularities at different radial positions other than curvature singularity at the origin. For this reason, this solution describes a bridge (known as wormhole) between two regions and electric flux crosses the bridge. Graves and Brill [143] investigated that the region of minimum radius (so called the "throat" of wormhole) contracts to non-zero radius and re-expands after some time due to electric field strength. Thus, unlike

the Schwarzschild solution, no particle can hit the singularity at $r = 0$ in RN solution.

These aspects of RN solution indicate that charge provides resistance (repulsion) against the gravitational collapse. Thus charge prevents the collapse of massive object to a singular point. This result was proved by Bonnor [144] while studying the physical properties of charged dust solution. He remarked that a charged dust ball with finite mass and small radius can remain in equilibrium against gravity by electrostatic repulsion provided by small amount of charge. This highly motivates to study the application of the Einstein-Maxwell field equations in relativistic gravitational collapse of the charged massive objects.

1.4 Spacetime Singularity

Spacetime singularity is one of the most important investigations of GR, developed during the dynamical evolution of the matter field in a spacetime. It is a point in spacetime where physical quantities such as energy density, spacetime curvature etc. become infinite and the usual laws of physics no longer hold. In general, singularities appear when solutions of the field equations are derived by imposing a high degree of symmetry on spacetime. It is of two types:

- Coordinate singularity;
- Essential or genuine singularity.

A singularity that occurs due to the bad choice of coordinates and can be removed by the change of coordinates is called *removable or coordinate singularity*. A singularity that cannot be removed is called *essential or*

genuine singularity. The essential singularity can further be divided into the following two types:

- Black hole;
- Naked singularity.

1.4.1 Black Hole

The region in spacetime where gravitational pull is so strong that even light cannot escape from it is called *black hole*. The boundary of BH is called *event horizon*. Black hole is formed when a massive star ($\gtrsim 10M_{\odot}$) undergoes to gravitational collapse and the resultant object has mass $\gtrsim 3.2M_{\odot}$. Black holes are complete collapsed and dense objects which have the following properties [3, 140]:

- The gravitational field of complete collapsed object is described by BH. This field can be characterized by three parameters that are mass M, charge Q and angular momentum Ma. The relationship between angular momentum and magnetic moment for a rotating BH is equivalent to that for electron.
- Black holes are surrounded by a surface, called *event horizon*, where gravitational field is so powerful that particles and light rays that once enter into the event horizon, can never escape and penetrate forever.
- At the end state of collapse, a genuine singularity of the gravitational field is produced that lies inside the event horizon of BH.
- Being a dense state of matter, a BH is stable and can never be destroyed by the external fields. Any form of matter entering from

outside into the BH can change its mass, charge and angular momentum.

- For all physical processes, the area of BH is non-decreasing. This statement is similar to the statement of the second law of thermodynamics, i.e., total entropy of all matter in the universe is non-decreasing.

1.4.2 Naked singularity

A spacetime singularity that can be observed by a far away observer is called *naked singularity*. This singularity is not covered by an event horizon and hence can be observed directly. Naked singularity has the following properties [145, 146]:

- A NS represents the formation of high curvature and strong gravity regions.
- Naked singularity provides source of gravitational waves.
- The amount of energy released during the formation of NS is less than the formation of BH, even collapsing stars have the same radius, mass and size.
- The information about the physics of quantum gravity can be obtained through the NS.

1.5 Cosmic Censorship Hypothesis

In 1969, Penrose [2] conjectured that the spacetime singularity (i.e., ultra dense region) resulting from the gravitational collapse of the generic matter

must be covered by an event horizon of gravity. In other words, gravitational collapse must end in a BH. This is known as *Cosmic Censorship Hypothesis*. However, there is no mathematical formulation for this hypotheis. It has the following two versions:

- Weak Cosmic Censorship Hypothesis (WCCH);
- Strong Cosmic Censorship Hypothesis (SCCH).

According to WCCH, there are certain classes of singularities forming at the end stage of gravitational collapse which are clothed by the event horizon and cannot be observed by an observer at infinity. In other words, the singularity may not be globally naked in gravitational collapse. The SCCH states that singularity can never be a locally naked at the end state of the collapse [145]. The mathematical conditions for the validity of two versions are entirely different. There are some models of collapse for which WCCH holds but SCCH is violated and vice versa.

1.6 Why Does Naked Singularity Form in Gravitational Collapse?

It is natural to ask what are the conditions under which a dynamical gravitational collapse ends as a NS. Matter is the only source of gravity in Newtonian theory, while in GR in addition to matter there is another factor known as spacetime curvature that plays vital role to determine the nature of gravitational field. The inhomogeneity in energy density and shear in matter distribution would delay the trapping of matter (as implied by the field equations), which can escape away from singularity. This implies

that the inhomogeneity in energy density creates path for matter to escape, leading to the formation of NS rather than BH.

When the amount of energy density inhomogeneity is very small (below a critical limit), a BH will form but for enough inhomogeneity, trapping of matter is delayed and as a result gravitational collapse will end as a NS [147]. Thus the presence of inhomogeneity is responsible for the formation of NS. If the density profile of the collapsed model is homogenous then the result would be a BH as in the case of Oppenheimer-Snyder model. Also, the density inhomogeneity of the collapsing matter delays the formation of horizons. If singularity forms earlier than horizons, the end state of collapse would be a NS.

1.7 Shell Focusing and Shell Crossing Singularities

The shell focusing singularities may occur when particles world-lines focus inwards to a point at the center of the collapsing star. These singularities may occur in TB spacetime where the family of radial null geodesics are incomplete and singularity cannot be removed by the extension of spacetime. The shell crossing singularities may arise from the crushing of matter shell of different radii around the center of spherical symmetry by forming a surface at which there would occur the intersection of light rays. It has been proved that such singularities can only occur when perfect fluid is considered as collapsing matter in the TB model [148, 149]. The spacetime can be extended through shell crossing singularities. The major property of these singularities is that the trajectories of the particles cross each other

at a single point.

1.8 Gravitational Strength of Singularity

The gravitational strength or strength of a singularity is a prominent feature of a singularity. A singularity is said to be *gravitationally strong* if it crushes or stretches to a zero volume of any massive object that falls on it. In case of Schwarzschild solution, singularity at $r = 0$ is a strong singularity [150]. The radially in-falling object is stretched infinitely in radial direction and is crushed to zero volume in tangential direction. On the other hand, a singularity is known as *weak singularity* if any object falling on it cannot be destroyed in this way.

The gravitational strength of a singularity is also directly related to the co-dimension of singularity. For four-dimensional spherically, cylindrically and plane symmetric spacetimes, there are point singularities, line singularities and plane singularities of co-dimension three, two and one, respectively [152]. It is well-known [153] that tidal forces for point singularities of co-dimension three are strong enough, so these can crush an object (falling onto singularities) to zero volume.

In GR, such singularities are clothed by event horizon. Also, tidal forces for line singularity are sufficiently strong (but weak as compared to point singularity) and can crush an object of finite size to zero volume (except conical singularity which is a famous example of cosmic string). Such singularities are naked if these are long and straight [154]. For plane singularities, the tidal forces are much weaker as compared to point and line singularities, so these cannot crush an object to a zero volume.

1.9 Spacelike and Timelike Singularities

A geodesically incomplete spacetime has a spacelike singularity in a region where timelike geodesics end. On the other hand, such spacetime has timelike singularity where the spacelike geodesics end up [155]. A spacelike singularity would protect CCH as such singularity guarantees the existence of event horizons whereas timelike singularity implies the existence of NS and hence violates CCH. It is well-known [1] that the Schwarzschild and FRW solutions have a spacelike singularity, while RN solution has a timelike singularity. The Kerr and Kerr-Newman metrics have also timelike nature, implying that nature of singularity explicitly depends upon the charge and rotation parameters of the collapsed object. This is an open issue to determine whether timelike singularities can be transformed into spacelike singularities by taking into account some realistic perturbations.

1.10 Trapped Surface

In 1965, Penrose introduced the concept of trapped surface in GR for the development of singularity theorems. A spacelike two-dimensional surface is called trapped surface if it satisfies the property that all the light rays directed outwards from this surface are convergent [156]. In spherical gravitational collapse, the presence of trapped surface would lead to the formation of BH if the collapsing matter satisfies the weak energy condition. In general, the trapped surfaces are formed during the gravitational collapse if sufficiently large matter is compacted into small volume. According to singularity theorems [1], if trapped surfaces exist then there must be a spacetime singularity to future. If one accepts the validity of CCH, then

the presence of trapped surfaces would lead to the indication that a BH is in the process of formation [157].

1.11 Event and Apparent Horizons

The BH region in a spacetime is a boundary from which no light ray can escape [158]. This boundary is called event horizon. In other words, the boundary of a region in spacetime that cannot be observed by a far away observer is called event horizon. According to Hawking and Ellis [1], event horizon is a null surface which can completely describe the causal structure of spacetime. In case of Schwarzschild BH, event horizon is at $r = 2m$.

Apparent horizon of a BH is the outer most boundary of a region that contains trapped surface. The gravitational collapse of a massive star which leads to the formation of BH, predicts that the event horizons are formed earlier than the apparent horizons [1]. The event horizon of a BH is not always the same as apparent horizon. Apparent horizon coincides with event horizon only for stationary spacetime [159]. If apparent horizon exists then it always lies inside the event horizon of BH.

1.12 Gravitational Lensing

Deflection of light rays by gravitational field is one of the consequences of GR. The phenomena resulting from the deflection of electromagnetic radiations in gravitational field is referred to *gravitational lensing* and an object causing a detectable deflection is known as *gravitational lens*. Firstly, Newton and Laplace discovered such deflection of light rays as these rays pass near massive bodies [160]. In 1804, Soldner [161] calculated the deflection

of light due to the Sun by assuming that light consists of material particles with Newtonian gravity. Later on, Einstein derived two formulae, one using the equivalence principle [162] and another on the basis of GR. He found that in the second case deflection angle is twice of the first case, which he remarked due to the curvature of gravitational lens [163]. According to the second formula, when a light ray tangentially grazes the surface of the Sun, it is deflected by $1.7''$.

1.13 The Cosmological Constant

Einstein believed that gravity contracts the universe. To overcome the attractive nature of gravity, Einstein introduced cosmological constant in his field equations that would act as repulsive nature of gravity. The cosmological constant was rejected by Einstein himself when Hubble discovered that the universe expands rather than contracts. Einstein admitted that the introduction of cosmological constant in the field equations was the biggest blunder of his life. However, the study of type Ia supernova [164] indicates that expansion of the universe is accelerating. To overcome this acceleration, it becomes necessary to add the cosmological constant in the field equations. The problems related to the growth, structure and age of the universe can be resolved by using cosmological constant in field equations [165]. The Einstein field equations with cosmological constant are given by

$$G_{\mu\nu} - \Lambda g_{\mu\nu} = \kappa T_{\mu\nu}, \tag{1.13.1}$$

where Λ is called cosmological constant. In the absence of matter, this reduces to

$$G_{\mu\nu} - \Lambda g_{\mu\nu} = 0. \tag{1.13.2}$$

1.14 Non-Commutative Theory of Gravity

In classical GR, singularity is such a region of spacetime at which the usual laws of physics break down. This problem can be removed by applying the formulation of NC field theory to GR [166]. For example, the NC BHs are one of the outcomes of string theory. These have such geometric structure in which curvature singularity is recovered by the minimal length introduced by the NC nature of coordinates. Further, all types of NC BHs expose the de-Sitter core due to quantum fluctuations at the center of the manifold.

The NC formulation of GR is one of the long standing problems which has no solution yet. The application of Moyal $\star$-product among the tetrad fields in the gravitational action is a mathematically correct approach but not physically. It is due to the fact that the expansion of $\star$-product in NC parameter is truncated upto a desirable order which causes to destroy the non-local nature of NC theory. This results to face the BH geometry with the same curvature singularities as in GR. Instead of using $\star$-product, one can formulate NC form of GR using the coordinate coherent state approach.

In this approach, the density of point like source in NC spacetime can be governed by a Gaussian distribution by using the relation [96]

$$\rho = \frac{e^{-\frac{r^2}{4\Theta^2}}}{(4\pi\Theta^2)^{\frac{d}{2}}}, \tag{1.14.1}$$

where d is the dimension of the manifold, Θ is constant having the dimension of length squared. Further, the correction to the field equations can be made by replacing the usual matter source by the Gaussian distribution while the curvature part of the field equations is left unchanged. Using this philosophy, many NC BH solutions have been derived [96]-[98]. Following this approach, we shall make only modification in matter part of the

junction conditions and leave the geometry part unchanged.

1.15 Boson Stars and Scalar Fields

The existence of dark matter has been demonstrated indirectly in various large scale structures in our universe, for example, from the individual galaxies to the whole universe [167]. Although, the direct measurements of the nature of dark matter have produced no significant result yet, but suppositions on its constituents deviate from baryonic matter to non-baryonic matter. One of the most reliable sources for dark matter is the boson star [168], which was discovered thirty years ago on the theoretical basis. The reality of boson stars have been applied successfully to several credible physical processes [169]. Such stars consist of real scalar fields which satisfy the Einstein-Klien-Gordon equations for the background geometry.

There are no evidences for the existence of real scalar fields in nature, but theoretically there are many arguments which explain the role of scalar fields in the structure formation and evolution of the universe. It is strongly believed that bosonic dark matter is collapsed to form boson stars. These are the static stars composed of zero temperature scalar particles. The existence of real scalar fields in GR was investigated by Wheeler and his collaborator [77, 78].

To discuss the physical aspects of boson star, Kaup [80], Ruffini and Bonazzola [81] found spherically symmetric solutions of the Einstein-Klein-Gordon equations. Further, they determined the equilibrium conditions for scalar field in boson stars. Also, these studies imply that scalar field configurations inside boson stars are macro quantum states and can be

prevented from gravitational collapse by Heisenberg uncertainty principle. Although, scalar fields are stable against the simple external perturbations but it is interesting to determine the stability conditions for the oscillating star in the presence of strong external perturbations.

1.16 Junction Conditions

After the discovery of the Schwarzschild interior and exterior solutions, the problem of junction conditions achieved a considerable interest in GR for matching two gravitational fields. In Newtonian physics for matching the two gravitational fields, boundary conditions, equation of continuity of gravitational potential and its first derivatives (when crosses the junction surface) were studied [170].

In contrast to Newtonian physics, GR is based on ideas that gravitational potential should be determined by the smoothness of the coordinates in which the metric of underlying geometry is described. The applications of junction conditions in GR commonly occur for studying the dynamics of matter thin shells, boundary of collapsing star, gravitational waves and cosmological phase transitions. In GR, the problem of smooth matching of two gravitational fields over a boundary surface was initially formulated by Lanczos [171, 172] which was generalized by several authors [52, 53, 173, 174].

To study the gravitational collapse of a star in GR, there are two versions of junctions conditions due to Darmois [173] and Israel [52, 53]. Both these require to consider the appropriate geometry of the interior and exterior regions of a star. For the smooth matching, a spacetime representing a

massive star is divided by a hypersurface Σ into two regions that are known as *interior and exterior spacetimes.*

For Darmois junction conditions in the interior spacetime, matter is considered, while the exterior spacetime is taken as vacuum (Schwarzschild), electro-vacuum (RN), or non-vacuum (Vaidya) if matter in the interior of a star is assumed to be perfect fluid, charged perfect fluid or heat conducting fluid. These usually determine the relation between the quantities of two regions over a boundary surface. For Israel junction conditions, both regions of a star are taken as vacuum and a thin layer of matter is considered on the boundary surface. These can be used as an alternative to the Einstein field equation for studying the dynamics of a system.

Darmois junction conditions are given as follows:

- The continuity of spacetimes over the hypersurface Σ gives

$$(ds_-^2)_\Sigma = (ds_+^2)_\Sigma = ds_\Sigma^2, \tag{1.16.1}$$

  where ds_-^2 and ds_+^2 represent the line elements of the interior and exterior spacetimes, respectively, ds_Σ^2 is the intrinsic metric defined on the hypersurface Σ. The subscript Σ indicates that these quantities must be evaluated at Σ.

- The continuity of the extrinsic curvature over the hypersurface Σ leads to

$$[K_{ij}] = K_{ij}^+ - K_{ij}^- = 0, \quad (i, j = 0, 2, 3), \tag{1.16.2}$$

  where K_{ij} is the extrinsic curvature which is given by

$$K_{ij}^\pm = -{n_\sigma}^\pm \left(\frac{\partial^2 x_\pm^\sigma}{\partial\xi^i \partial\xi^j} + \Gamma_{\mu\nu}^\sigma \frac{\partial {x_\pm}^\mu}{\partial\xi^i} \frac{\partial {x_\pm}^\nu}{\partial\xi^j}\right). \tag{1.16.3}$$

Here n_σ is normal to the boundary surface given by

$$n_\sigma = \frac{f_{,\sigma}}{|g^{\nu\lambda} f_{,\nu} f_{,\lambda}|^{\frac{1}{2}}}, \tag{1.16.4}$$

where $f = 0$, defines the equation of hypersurface Σ. The Israel junction conditions require the continuity of the line elements, while the second condition is modified as follows [52]

$$S_{ij} = \frac{1}{\kappa}\{[K_{ij}] - \gamma_{ij}[K]\}, \tag{1.16.5}$$

where S_{ij} is the surface energy-momentum tensor, κ is the coupling constant, γ_{ij} is the induced metric on Σ and

$$[K_{ij}] = K^+_{ij} - K^-_{ij}, \qquad [K] = \gamma^{ij}[K_{ij}]. \tag{1.16.6}$$

Chapter 2

Charged Perfect Fluid Cylindrical Gravitational Collapse

In this chapter, we investigate charged perfect fluid cylindrical gravitational collapse. For this purpose, we determine analytic solution of the Einstein-Maxwell field equations by assuming that charged perfect fluid is moving along the geodesics in the interior of cylinder. This assumption implies that $g_{00} = 1$ for the underlying metric. Recently, Brandt et al. [175] have studied spherically symmetric perfect fluid gravitational collapse with geodesic assumption.

In the present chapter, we use the geodesic assumption and explore analytic solution of the field equations with charged perfect fluid in cylindrically symmetric spacetime. We find that solution represents gravitational collapse of cylinder along the longitudinal direction. This chapter is organized as follows. We explore the solution of the Einstein-Maxwell field equations in section **2.1**. The physical properties of the solutions are discussed in section **2.2**. Section **2.3** is devoted to study the junction conditions between the interior charged perfect solution and exterior charged vacuum solution. Results of this chapter have been published in the form of a research paper

[176].

2.1 Solution of Einstein-Maxwell Field Equations

This section is devoted to investigate solution of the Einstein-Maxwell field equations coupled with perfect fluid as the source of gravitation distributed per unit length of the cylinder. The general cylindrically symmetric spacetime is given by the following line element [177]

$$ds^2_- = A^2(dt^2 - dr^2) - B^2 d\theta^2 - C^2 dz^2, \tag{2.1.1}$$

where A, B and C are functions of t and r. Here, we take the following restrictions on the coordinates in order to preserve the cylindrical symmetry of the spacetime

$$-\infty < t < \infty, \quad 0 \leq r, \quad 0 \leq \theta \leq 2\pi, \quad -\infty < z < \infty. \tag{2.1.2}$$

The proper unit length of the cylinder for the line element (2.1.1) is defined by

$$l = 2\pi BC. \tag{2.1.3}$$

For the solution of Einstein-Maxwell field equations, we have to solve the Maxwell equations (1.2.9) with Maxwell field tensor (1.2.2) for the line element (2.1.1). For this purpose, we assume that in comoving coordinates system, the charge per unit length of the cylinder is at rest so that the magnetic field will be zero. Thus we can choose four potential and four current as follows

$$\phi_\mu = (\phi(t, r), 0, 0, 0), \quad J^\mu = \sigma u^\mu, \tag{2.1.4}$$

where σ is the charge density. The only non-zero component of the Maxwell field tensor is

$$F_{01} = -F_{10} = -\frac{\partial \phi}{\partial r}. \tag{2.1.5}$$

Thus the Maxwell equations (1.2.9) take the following form

$$\frac{1}{A^3}\frac{\partial^2 \phi}{\partial r^2} + \frac{1}{A^3}\frac{\partial \phi}{\partial r}\left(\frac{B'}{B} + \frac{C'}{C} - 2\frac{A'}{A}\right) = 4\pi\sigma, \tag{2.1.6}$$

$$\frac{1}{A^4}\left(\frac{\partial^2 \phi}{\partial t \partial r} + \frac{\partial \phi}{\partial r}(\frac{\dot{B}}{B} + \frac{\dot{C}}{C} + 2\frac{\dot{A}}{A})\right) + \frac{\partial}{\partial t}(\frac{1}{A^4})\frac{\partial \phi}{\partial r} = 0, \tag{2.1.7}$$

where dot and prime indicate derivatives with respect to time t and radial coordinate r, respectively. Integration of Eq.(2.1.6) implies that

$$\frac{\partial \phi}{\partial r} = \frac{2qA^2}{BC}, \tag{2.1.8}$$

where $q(r) = 2\pi \int_0^r \sigma(ABC)dr$ is the total amount of charge per unit length of the cylinder. We would like to mention here that Eq.(2.1.7) is satisfied by Eq.(2.1.8). Equation (2.1.5) can also be written as

$$F_{01} = -F_{10} = -\frac{2qA^2}{BC}. \tag{2.1.9}$$

The non-zero components of $T_\mu^{\nu(em)}$ turn out to be

$$T_0^{0(em)} = T_1^{1(em)} = -T_2^{2(em)} = -T_3^{3(em)} = \frac{1}{2\pi}\frac{q^2}{(BC)^2}.$$

The electric field intensity is defined by

$$E(r,t) = \frac{q}{2\pi(BC)}. \tag{2.1.10}$$

The energy-momentum tensor for perfect fluid is

$$T_{\mu\nu} = (\rho + p)u_\mu u_\nu - p g_{\mu\nu}, \tag{2.1.11}$$

where ρ is the energy density, p is the pressure and $u_\mu = A\delta_\mu^0$ is the four-vector velocity in comoving coordinates.

The Einstein-Maxwell field equations (1.3.1) for cylindrically symmetric perfect fluid distribution take the following form

$$-\frac{B''}{B}-\frac{C''}{C}+\frac{A'}{A}\left(\frac{B'}{B}+\frac{C'}{C}\right)+\frac{\dot{A}}{A}\left(\frac{\dot{B}}{B}+\frac{\dot{C}}{C}\right)-\frac{B'C'}{BC}+\frac{\dot{B}\dot{C}}{BC}$$
$$=8\pi A^2\left(\rho+\frac{q^2}{2\pi B^2C^2}\right), \tag{2.1.12}$$
$$-\frac{\dot{B}'}{B}+\frac{\dot{C}'}{C}+\frac{\dot{A}}{A}\left(\frac{\dot{B}}{B}+\frac{\dot{C}}{C}\right)-\frac{\dot{A}}{A}\left(\frac{B'}{B}+\frac{C'}{C}\right)=0, \tag{2.1.13}$$
$$\frac{A'}{A}(\frac{B'}{B}+\frac{C'}{C})+\frac{\dot{A}}{A}\left(\frac{\dot{B}}{B}+\frac{\dot{C}}{C}\right)+\frac{B'C'}{BC}+\frac{\dot{B}\dot{C}}{BC}-\frac{\ddot{B}}{B}-\frac{\ddot{C}}{C}$$
$$=8\pi A^2\left(p-\frac{q^2}{2\pi B^2C^2}\right), \tag{2.1.14}$$
$$-\frac{\ddot{C}}{C}+\frac{C''}{C}+\left(\frac{A'}{A}\right)'-(\frac{\ddot{A}}{A})+\frac{\dot{A}}{A^2}=8\pi A^2\left(p+\frac{q^2}{2\pi B^2C^2}\right), \tag{2.1.15}$$
$$-\frac{\ddot{B}}{B}+\frac{B''}{B}+\left(\frac{A'}{A}\right)'-(\frac{\ddot{A}}{A})+\frac{\dot{A}}{A^2}=8\pi A^2\left(p+\frac{q^2}{2\pi B^2C^2}\right). \tag{2.1.16}$$

We assume that the charged perfect fluid distributed per unit length of the cylinder follows along the geodesics in the interior of cylinder. This requires that velocity should be uniform and acceleration must be zero which is only possible if A is constant (for simplicity, we take $A=1$). Thus using Eq.(2.1.10), we can rewrite Eqs.(2.1.12)-(2.1.16) as follows

$$-\frac{B''}{B}-\frac{C''}{C}+\frac{\dot{C}}{C}-\frac{B'C'}{BC}+\frac{\dot{B}\dot{C}}{BC} = 8\pi\left(\rho+2\pi E^2\right), \tag{2.1.17}$$
$$\frac{\dot{B}'}{B}+\frac{\dot{C}'}{C} = 0, \tag{2.1.18}$$
$$\frac{B'C'}{BC}-\frac{\dot{B}\dot{C}}{BC}-\frac{\ddot{B}}{B}-\frac{\ddot{C}}{C} = 8\pi\left(p-2\pi E^2\right), \tag{2.1.19}$$
$$-\frac{\ddot{C}}{C}+\frac{C''}{C} = 8\pi\left(p+2\pi E^2\right), \tag{2.1.20}$$
$$-\frac{\ddot{B}}{B}+\frac{B''}{B} = 8\pi\left(p+2\pi E^2\right). \tag{2.1.21}$$

We note that there are five equations and five unknowns $B,\ C,\ p,\ \rho,\ E$, therefore we can find a unique solution.

For this purpose, we adopt the method of separation of variables. The comparison of Eqs.(2.1.20) and (2.1.21) gives

$$-\frac{\ddot{C}}{C}+\frac{C''}{C}=-\frac{\ddot{B}}{B}+\frac{B''}{B}. \tag{2.1.22}$$

Let

$$B(t,r)=f(r)g(t), \quad C(t,r)=h(r)k(t). \tag{2.1.23}$$

Using Eq.(2.1.23) in (2.1.18), we get

$$f=\alpha h^{L}, \quad k=\delta g^{-L}, \tag{2.1.24}$$

where L ($\neq 0$, for non-trivial solution) is a separation constant while α and δ are integration constants. Using Eq.(2.1.24) in (2.1.22), it follows that

$$\frac{\ddot{g}}{g}-\frac{\ddot{k}}{k}=\frac{f''}{f}-\frac{h''}{h}. \tag{2.1.25}$$

Since both sides are functionally independent, we put them equal to constant say $M(\neq 0)$

$$\frac{\ddot{g}}{g}-\frac{\ddot{k}}{k}=M=\frac{f''}{f}-\frac{h''}{h}. \tag{2.1.26}$$

Application of Eq.(2.1.24) to (2.1.26) leads to

$$\frac{\ddot{g}}{g}-\frac{\dot{g}^2}{g^2}=\frac{M}{L+1}, \quad \frac{h''}{h}+\frac{h'^2}{h^2}=\frac{M}{L-1}. \tag{2.1.27}$$

The solution of these equations is

$$g(t)=\beta_0\cos^{\frac{1}{1-L}}(W(t+t_0)), \quad h(r)=\beta_1\cosh^{\frac{1}{1+L}}(S(r+r_0)), \tag{2.1.28}$$

where $\beta_0,\ \beta_1,\ t_0$ and r_0 are constants of integration. Further, W and S are given by the following relations

$$W=\sqrt{\frac{M(L-1)}{L+1}}, \quad S=\sqrt{\frac{M(L+1)}{L-1}}. \tag{2.1.29}$$

Using Eq.(2.1.28) in (2.1.24), it follows that

$$k(t)=\beta_2\cos^{\frac{L}{L-1}}(W(t+t_0)),\quad f(r)=\beta_3\cosh^{\frac{L}{1+L}}(S(r+r_0)),\quad (2.1.30)$$

where β_2 and β_3 are constants of integration. Thus the metric coefficients, given by Eq.(2.1.23), turn out to be

$$B=\Omega\cosh^{\frac{L}{1+L}}(S(r+r_0))\cos^{\frac{1}{1-L}}(W(t+t_0)),\qquad (2.1.31)$$

$$C=\Psi\cosh^{\frac{1}{1+L}}(S(r+r_0))\cos^{\frac{L}{L-1}}(W(t+t_0)),\qquad (2.1.32)$$

where $\Omega=\beta_0\beta_3,\ \Psi=\beta_1\beta_2$. Consequently, the spacetime (2.1.1) takes the form

$$\begin{aligned} ds^2_- &= dt^2-dr^2-\Omega^2\cosh^{\frac{2L}{1+L}}(S(r+r_0))\cos^{\frac{2}{1-L}}(W(t+t_0))d\theta^2 \\ &- \Psi^2\cosh^{\frac{2}{1+L}}(S(r+r_0))\cos^{\frac{2L}{L-1}}(W(t+t_0))dz^2. \qquad (2.1.33)\end{aligned}$$

Using the following transformations

$$Sr'=S(r+r_0),\quad Wt'=W(t+t_0),\quad \theta'=\Omega\theta,\quad z'=\Psi z,$$

the above metric (2.1.33) reduces to

$$\begin{aligned} ds^2_- &= dt'^2-dr'^2-\cosh^{\frac{2L}{1+L}}(Sr')\cos^{\frac{2}{1-L}}(Wt')d\theta'^2 \\ &- \cosh^{\frac{2}{1+L}}(Sr')\cos^{\frac{2L}{L-1}}(Wt')dz'^2. \qquad (2.1.34)\end{aligned}$$

By assuming $\Omega=1$, it is clear that the above metric preserves cylindrical symmetry with the restriction on coordinates given by Eq.(2.1.2). We take

$$\tilde{B}=\cosh^{\frac{L}{1+L}}(Sr')\cos^{\frac{1}{1-L}}(Wt'),\quad \tilde{C}=\cosh^{\frac{1}{1+L}}(Sr')\cos^{\frac{L}{L-1}}(Wt').$$

2.2 Physical Properties of the Solution

Here, we discuss some physical and geometrical properties of the solution. The physical parameters, i.e., pressure p, density ρ, and the electric field

intensity E are given by

$$p = \frac{1}{16\pi}\left[\frac{S^2}{(1+L)} - \frac{4\tan^2(Wt')W^2L}{(1-L)^2} + \frac{W^2}{(L-1)(2L-1)}\right], \quad (2.2.1)$$

$$E = \left[\frac{1}{32\pi^2}\left(\frac{2L(1+L)^2W^2\sec^2(Wt') - (1+L)^3W^2 - (L-1)^3S^2}{(1-L^2)^2}\right.\right.$$
$$\left.\left. + \frac{2LS^2\sec^2h(Sr')}{(L+1)^2}\right)\right]^{\frac{1}{2}}, \quad (2.2.2)$$

$$\rho = \frac{1}{8\pi}\left[\frac{-S^2(1+L+L^2+L\sec^2h(Sr'))}{(L+1)^2} + \frac{LW^2\tan^2(Wt')}{(L-1)^2}\right]. \quad (2.2.3)$$

We would like to mention here that Eqs.(2.1.31), (2.1.32) and (2.2.1)-(2.2.3) satisfy all the field equations with the restriction on constants given by Eq.(2.1.29). The proper unit length of the cylinder for the new metric is given by

$$l = 2\pi\tilde{B}\tilde{C} \equiv 2\pi\cosh(Sr')\cos(Wt') \quad (2.2.4)$$

and the longitudinal length in this case is

$$\tilde{l} = \frac{l}{2\pi} = \tilde{B}\tilde{C} \equiv \cosh(Sr')\cos(Wt'). \quad (2.2.5)$$

The rate of change of longitudinal length is

$$\dot{\tilde{l}} = -W\cosh(Sr')\sin(Wt'), \quad (2.2.6)$$

where negative sign shows that motion is directed inward. Such motion represents gravitational collapse of the charged perfect fluid distributed per unit length of the cylinder.

In order to analyze the nature of singularity of the solution, we use curvature invariants. Many scalars can be constructed from the Riemann tensor but symmetry assumption can be used to find only a finite number of independent scalars. Some of these are

$$R_1 = R = g^{ab}R_{ab}, \quad R_2 = R_{ab}R^{ab}, \quad R_3 = R_{abcd}R^{abcd}, \quad R_4 = R^{ab}_{cd}R^{cd}_{ab}.$$

Here, we give the analysis for the first invariant commonly known as the Ricci scalar. For the metric (2.1.34), it is given by

$$R = \frac{2}{\tilde{l}}(\ddot{\tilde{B}}\tilde{C} - \tilde{B}\ddot{\tilde{C}} - \tilde{B}''\tilde{C} - \tilde{C}''\tilde{B} + \dot{\tilde{B}}\dot{\tilde{C}} - \tilde{B}'\tilde{C}'). \tag{2.2.7}$$

We see that the Ricci scalar as well as all the other curvature invariants and physical parameters of the solution are finite for $r' \to 0$. Thus $r' = 0$ is the conical singularity of the new metric.

Now we analyze values of the constants for which the solution is physical. In this solution, L and M are non-zero separation constants for the non-trivial solution, while the rest are integration constants that can be removed by applying the transformations to Eq.(2.1.33) and by evaluating the physical parameters from the field equations. From Eq.(2.1.29), it is clear that the constants W and S cannot be chosen arbitrarily. These are non-zero because $M \neq 0$ for non-trivial solution. Further, for W and S to be real, we have the following four possible solutions

$$1. \quad L < -1, \quad M > 0; \quad 2. \quad L > -1, \quad M < 0;$$
$$3. \quad L > 1, \quad M > 0; \quad 4. \quad L < 1, \quad M < 0.$$

Keeping in mind these restrictions on the constants, we find that the cases **1** and **2** lead to non-physical solutions (i.e., negative energy density for the arbitrary choice of coordinates). In the case **3**, for $0 < M \leq 0.5$ and $1 < L \leq 1.9$, there exists a physical solution which represents gravitational collapse. The graphs **2.1-2.4** in this case indicate that all the physical quantities become homogeneous. Thus the geodesic model with charged perfect fluid distributed per unit length of the cylinder is free of initial inhomogeneities.

It is interesting to mention here that pressure remains a function of time only for this geodesic model that is analogous to the spherical case [175]. In the case **4** for $0.63 \leq L \leq 0.95$ and $-1 < M \leq -0.10$, all quantities except pressure behave like the case **3**, while pressure is negative in this case indicating a DE solution. As long as the realistic energy condition $\rho + 3p > 0$ holds, gravity remains attractive. However, the violation of this condition, i.e., $\rho + 3p < 0$ due to negative pressure, leads to the repulsive gravitational effects. Thus in the relativistic physics, negative pressure acting as a repulsive gravity plays the role of preventing the gravitational collapse. We are interested to study the gravitational collapse which is the consequence of attractive gravity, so the case **4** leads to expanding solution. Thus the only case **3** is interesting for gravitational collapse.

The rate of change of longitudinal length in Figure **2.1** shows that the longitudinal length is a decreasing function of time, thus the resulting solution represents the gravitational collapse. The collapse starts at some finite time and ends at $t' = 1$, where longitudinal length of the cylinder reduces to zero. Further, energy density is an increasing function of time shown in Figure **2.2**. This is the strong argument for a model to represent collapse. The pressure in the interior of cylinder starts decreasing as shown in Figure **2.3**. This causes to initiate the gravitational collapse, more matter is concentrated in the small volume, hence density goes on increasing.

It is to be noted that decrease in the proper unit length of the cylinder, increases the interaction between the electric charges and a strong electromagnetic force inside the cylinder is created. This is an increasing function of time as shown in Figure **2.4**. The resultant action of electromagnetic and gravitational forces play a dominant role to reduce longitudinal length

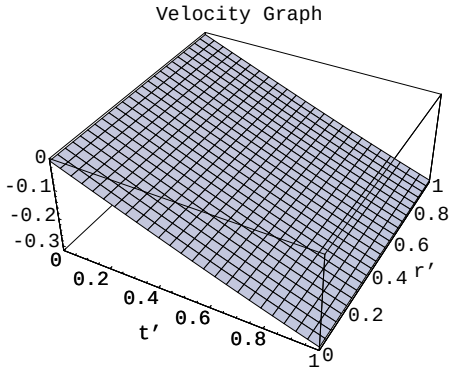

Figure 2.1: Decrease in longitudinal length with the passage of time for $0 < M \leq 0.5$ and $1 < L \leq 1.9$.

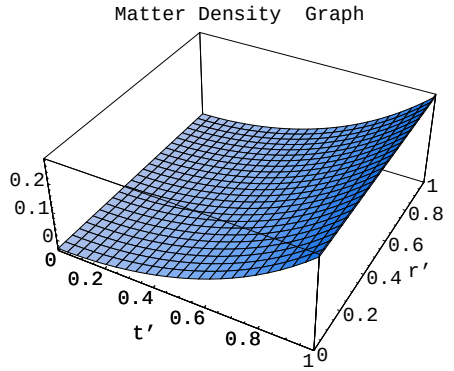

Figure 2.2: Increase in density with the passage of time for $0 < M \leq 0.5$ and $1 < L \leq 1.9$.

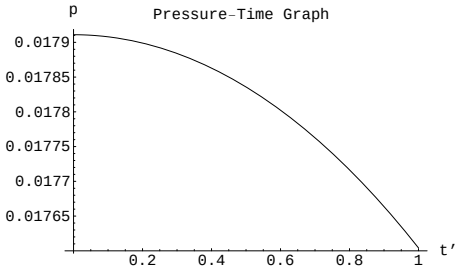

Figure 2.3: Decrease in pressure with the passage of time for $0 < M \leq 0.5$ and $1 < L \leq 1.9$

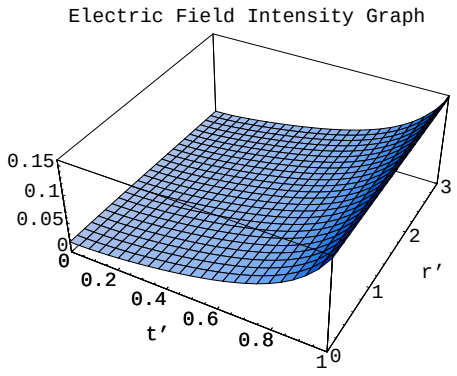

Figure 2.4: Increase in electric intensity with the passage of time for $0 < M \leq 0.5$ and $1 < L \leq 1.9$.

of cylinder to zero.

The nature of the collapse can be explained as follows. When latitudinal and vertical lengths of the cylinder reduce to zero, there is a complete collapse. From the metric (2.1.33), we have $g_{\theta\theta} = \tilde{B}^2$, $g_{zz} = \tilde{C}^2$. Since singularity analysis implies that the Ricci scalar diverges at a point where the longitudinal length is zero. Thus when the longitudinal length as well as the latitudinal and vertical lengths reduce to zero, we obtain a conical singularity at $r' = 0$.

2.3 Junction Conditions

We assume that the 3D spacelike boundary surface Σ splits the two 4D cylindrically symmetric spacetimes M^+ and M^-. The metric which describes the internal region M^- is the charged perfect fluid solution given by Eq.(2.1.34). For the exterior region M^+, a charged cylindrically symmetric electro-vacuum solution is taken as [178]

$$ds_+^2 = ZdT^2 - \frac{1}{Z}dR^2 - R^2(d\theta^2 + \alpha^2 dz^2), \tag{2.3.1}$$

where $Z(R) = \frac{2Q^2}{R^2} - \frac{4m}{R}$, α is constant with the dimension of $\frac{1}{length}$, m and Q are the mass and charge distributed per unit length of the cylinder, respectively. This choice of the exterior solution in M^+ region is compatible with the charged perfect fluid solution in the interior region M^- for the smooth matching over the boundary surface Σ.

The boundary surface Σ in terms of interior and exterior coordinates can be described by the following equations

$$k_-(r', t') = \quad r' - r'_\Sigma = 0, \tag{2.3.2}$$

$$k_+(R, T) = \quad R - R_\Sigma(T) = 0, \tag{2.3.3}$$

where r'_Σ is a constant. Using these equations, the interior and exterior metrics on Σ take the following form

$$(ds^2_-)_\Sigma = dt'^2 - \tilde{B}^2 d\theta'^2 - \tilde{C}^2 dz'^2, \tag{2.3.4}$$

$$(ds^2_+)_\Sigma = [Z(R_\Sigma) - \frac{1}{Z(R_\Sigma)}(\frac{dR_\Sigma}{dT})^2]dT^2 - R^2_\Sigma(d\theta^2 + \alpha^2 dz^2). \tag{2.3.5}$$

Here we assume $g_{00} > 0$ so that T is a timelike coordinate. Also, from Eqs.(1.16.4), (2.3.2) and (2.3.3), the outward unit normals from boundary surface Σ to interior and exterior regions are given by

$$n^-_\mu = (0, 1, 0, 0), \quad n^+_\mu = (-R^\dagger{}_\Sigma, T^\dagger, 0, 0), \tag{2.3.6}$$

where dagger $\dagger$ represents derivatives with respect to new coordinate t'.

The continuity of the first fundamental form from Eq.(1.16.2) over Σ gives

$$\begin{aligned} &(\tilde{B})_\Sigma = R_\Sigma, \quad (\tilde{C})_\Sigma = \alpha R_\Sigma, \quad \Longrightarrow \quad (\tilde{C})_\Sigma = \alpha(\tilde{B})_\Sigma, \\ &[Z(R_\Sigma) - \frac{1}{Z(R_\Sigma)}(\frac{dR_\Sigma}{dT})^2]^{\frac{1}{2}} dT = (dt')_\Sigma. \end{aligned} \tag{2.3.7}$$

From Eq.(1.16.3), the components of extrinsic curvature $K_{ij}^{\pm}$ in terms of interior and exterior coordinates are

$$\begin{aligned} K_{00}^{-} &= 0, \quad K_{22}^{-} = \frac{1}{\alpha^2} K_{33}^{-} = (\tilde{B}\bar{\tilde{B}})_{\Sigma}, \\ K_{00}^{+} &= (R^{\dagger}T^{\dagger\dagger} - T^{\dagger}R^{\dagger\dagger} - \frac{Z}{2}\frac{dZ}{dR}T^{\dagger\dagger 3} + \frac{3}{2Z}\frac{dZ}{dR}T^{\dagger}R^{\dagger^2})_{\Sigma}, \\ K_{22}^{+} &= \frac{1}{\alpha^2} K_{33}^{+} = (ZRT^{\dagger})_{\Sigma}, \end{aligned} \tag{2.3.8}$$

where bar $^{-}$ represents differentiation with respect to the new coordinate r'.

Also, the continuity of the extrinsic curvature components from Eq.(1.16.3) with Eqs.(2.3.7) and (2.3.8) leads to

$$(\bar{\tilde{B}}^{\dagger})_{\Sigma} = 0, \tag{2.3.9}$$

$$m = [\frac{Q^2}{2\tilde{B}} + \frac{\tilde{B}}{4}(\tilde{B}^{\dagger 2} - \bar{\tilde{B}}^2)]_{\Sigma}. \tag{2.3.10}$$

Equation.(2.3.9) implies that the boundary surface Σ represents a cylinder with constant proper unit length which behaves as boundary of the interior charged perfect fluid. It connects the interior charged perfect fluid solution to the exterior electro-vacuum solution. Using Eq.(2.3.9) in (2.3.10), we get $m = (\frac{Q^2}{2\tilde{B}})_{\Sigma}$. This equation implies that gravitational and Coulomb forces of the system balance each other on the boundary surface Σ.

Chapter 3

Scalar Field and Polytropic Matter Thin Shell Collapse in Charged Background

This chapter is devoted to explore the dynamics of scalar field and polytropic matter thin shell in RN geometry. For this purpose, we derive the general equations of motion for thin shell by using Israel formalism, then apply these equations to scalar field and polytropic matter thin shell. This chapter generalizes the dynamics of scalar field thin shell by Núñez et al. [94] and polytropic matter thin shell by Oh and Park [102] from the Schwarzschild geometry to RN geometry.

We divide this chapter into three main sections. In section **3.1**, we formulate the general equations of motion by taking interior and exterior regions of a star as RN geometries. The boundary surface (between the interior and exterior regions of a star) representing the thin layer of matter is taken as spacelike 3D surface. Section **3.2** is devoted to discuss the dynamics of scalar field by considering the massless and massive scalar field cases explicitly. The polytropic matter as well as perfect fluid thin shell collapse is presented in section **3.3**. Further, the effects of NC parameter on the collapse of polytropic matter and perfect fluid shell are investigated.

Throughout this chapter, equations of motion are solved numerically. We have published two research papers [179, 180] on the basis of results presented in this chapter.

3.1 Equations of Motion in Charged Background

In this section, we use Israel thin shell formulation to derive equations of motion for thin shell of matter. We take a 3D spacelike boundary surface Σ, which splits the two 4D spherically symmetric spacetimes M^+ and M^-. The exterior and interior regions $M^+$and M^-, respectively are described by the RN metrics given by

$$(ds)^2_\pm = N_\pm dT^2 - \frac{1}{N_\pm} dR^2 - R^2(d\theta^2 + \sin^2\theta d\phi^2), \tag{3.1.1}$$

where $N_\pm(R) = 1 - \frac{2M_\pm}{R} + \frac{Q^2_\pm}{R^2}$, $M_\pm$ and $Q_\pm$ are the mass and charge, respectively. The subscripts $+$ and $-$ represent quantities in exterior and interior regions to Σ, respectively. Further, it is assumed that charge in both regions is the same, i.e., $Q_+ = Q_- = Q$. The strength of electric field on the shell can be described by the Maxwell field tensor, $F_{TR} = \frac{Q}{R^2} = -F_{RT}$.

By employing the intrinsic coordinates (τ, θ, ϕ) on Σ at $R = R(\tau)$, the metrics (3.1.1) on Σ become

$$(ds)^2_{\pm\Sigma} = [N_\pm(R) - \frac{1}{N_\pm(R)}(\frac{dR}{d\tau})^2(\frac{d\tau}{dT})^2]dT^2 - R^2(\tau)(d\theta^2 + \sin^2\theta d\phi^2). \tag{3.1.2}$$

Here, it is assumed that $g_{00} > 0$ so that T is a timelike coordinate. Also, the induced metric on the boundary surface Σ is given by

$$(ds)^2_\Sigma = d\tau^2 - a^2(\tau)(d\theta^2 + \sin^2\theta d\phi^2). \tag{3.1.3}$$

The continuity of the first fundamental form gives

$$[N_{\pm}(R_{\Sigma}) - \frac{1}{N_{\pm}(R_{\Sigma})}(\frac{dR_{\Sigma}}{d\tau})^2(\frac{d\tau}{dT})^2]^{\frac{1}{2}}dT = (d\tau)_{\Sigma}, \quad R(\tau) = a(\tau)_{\Sigma}. \quad (3.1.4)$$

The outward unit normals ${n_{\mu}}^{\pm}$ to Σ in $M^{\pm}$ coordinates can be evaluated as

$${n_{\mu}}^{\pm} = (-\dot{R}(\tau), \dot{T}, 0, 0), \quad (3.1.5)$$

where dot represents differentiation with respect to τ.

The non-vanishing components of the extrinsic curvature are

$$K^{\pm}_{\tau\tau} = \frac{d}{dR}\sqrt{\dot{R}^2 + N_{\pm}}, \quad K^{\pm}_{\theta\theta} = -R\sqrt{\dot{R}^2 + N_{\pm}}, \quad K^{\pm}_{\phi\phi} = K^{\pm}_{\theta\theta}\sin^2\theta. \quad (3.1.6)$$

The perfect fluid energy-momentum tensor is

$$S_{ij} = (\rho + p)u_i u_j - p\gamma_{ij}, \quad (3.1.7)$$

where $u_i = \delta^0_i$ and γ_{ij} is same defined after Eq.(1.16.5) . Using Eqs.(3.1.4), (3.1.7) and (1.16.5) and (1.16.6), we obtain

$$\rho = \frac{2}{\kappa R^2}[K_{\theta\theta}], \quad p = \frac{1}{\kappa}\{[K_{\tau\tau}] - \frac{[K_{\theta\theta}]}{R^2}\}. \quad (3.1.8)$$

Inserting the non-zero components of the extrinsic curvature components, we get

$$(\eta_+ - \eta_-) + \frac{\kappa}{2}\rho R = 0, \quad (3.1.9)$$

$$\frac{d}{dR}(\eta_+ - \eta_-) + \frac{1}{R}(\eta_+ - \eta_-) - \kappa p = 0, \quad (3.1.10)$$

where $\eta_{\pm} = \sqrt{\dot{R}^2 + N_{\pm}}$.

Making use of Eq.(3.1.9) in (3.1.10), it follows that

$$\frac{d\rho}{dR} + \frac{2}{R}(p + \rho) = 0. \quad (3.1.11)$$

Alternatively, it can also be written as

$$\dot{m} + p\dot{A} = 0, \tag{3.1.12}$$

where $m(= \rho A)$ and $A(= 4\pi R^2(\tau))$ stand for the integrated total energy density at some time and area of the shell, respectively. The conservation of surface energy-momentum tensor leads to the same equation as Eq.(3.1.12), hence this equation is known as energy conservation law on the shell.

Equation (3.1.11) can be solved by using EoS, $p = k\rho$, yielding the solution

$$\rho = \rho_0(\frac{R_0}{R})^{2(k+1)}, \tag{3.1.13}$$

where R_0 is the position of the shell at $\tau = \tau_0$ and ρ_0 is the density of matter on the shell at position R_0. Inserting this value of ρ in the definition of m, we get

$$m = 4\pi\rho_0 \frac{R_0^{(2k+2)}}{R^{2k}}. \tag{3.1.14}$$

From Eq.(3.1.9), we obtain equation of motion of thin shell given by

$$\dot{R}^2 + V_{eff}(R) = 0, \tag{3.1.15}$$

where the effective potential $V_{eff}(R)$ is

$$V_{eff}(R) = \frac{1}{2}(N_+ + N_-) - \frac{(N_+ - N_-)^2}{(\kappa\rho R)^2} - \frac{1}{16}(\kappa\rho R)^2. \tag{3.1.16}$$

Alternatively, it can be written in the following form

$$V_{eff}(R) = 1 - \left(\frac{M_+ - M_-}{m}\right)^2 + \left(\frac{Q}{R}\right)^2 - \frac{(M_+ + M_-)}{R} - \left(\frac{m}{2R}\right)^2, \tag{3.1.17}$$

where we have used $\kappa = 8\pi$.

To see the effects of charge parameter Q on the dynamics of the shell, we can write Eq.(3.1.15) by using the above equation as follows

$$\dot{R} = \pm\sqrt{\left(\frac{M_+ - M_-}{m}\right)^2 - \left(\frac{Q}{R}\right)^2 + \frac{(M_+ + M_-)}{R} + \left(\frac{m}{2R}\right)^2 - 1.} \tag{3.1.18}$$

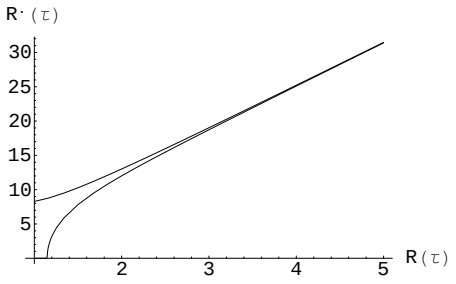

Figure 3.1: Behavior of the shell velocity with respect to stationary observer, when $M_+ = 1,\ M_- = 0,\ k = \rho_0 = R_0 = 1$ and $Q = 1$. The upper and lower curves correspond to uncharged and charged cases, respectively. It is clear that initially velocity in the charged case is less than the uncharged case. Velocity in both cases match for larger values of R as the term $\frac{Q^2}{R^2}$ becomes negligible.

Here $+(-)$ correspond to expansion (collapse) of the shell and m is the same as defined after Eq.(3.1.12). The term $\frac{Q^2}{R^2}$ (Coulomb repulsive force) in $\dot{R}$ (velocity of the shell with respect to stationary observer) indicates that charge reduces shell velocity with respect to stationary observer. This velocity also depends on position of the observer, whether the observer is located inside or outside the shell. Further, Eq.(3.1.17) implies that charge parameter increases the effective potential V_{eff}.

In next sections, we shall see that throughout the dynamics of the shell, charge parameter reduces the velocity of the shell with respect to stationary observer. Thus initially the velocity of the shell with respect to stationary observer in the RN background is slower as compared to the Schwarzschild case (as shown in Figure **3.1**). We conclude that electrostatic repulsive force in RN background tries to balance with the gravitational force due to the shell and hence the shell velocity with respect to stationary observer is slow in charged case as compared to the uncharged case.

3.2 Scalar Field Thin Shell Collapse

In order to study the dynamics of scalar field thin shell, we apply a transformation on the perfect fluid energy-momentum tensor, so that we have a scalar field energy-momentum tensor. The transformation is [94]

$$u_i = \frac{\phi_{,i}}{\sqrt{\phi_{,j}\phi^{,j}}}, \quad \rho = \frac{1}{2}[\phi_{,\ \nu}\phi^{,\ \nu} + 2V(\phi)],\ p = \frac{1}{2}[\phi_{,\ \nu}\phi^{,\ \nu} - 2V(\phi)], \tag{3.2.1}$$

where $V(\phi) = \tilde{m}^2\phi^2$ is the potential term which is non-zero for massive scalar field. We note that the scalar field will be massless in the absence of such term. Using Eqs.(3.1.7) and (3.2.1), we can write the energy-momentum tensor of the scalar field as follows

$$S_{ij} = \nabla_i\phi\nabla_j\phi - \gamma_{ij}\ [\frac{1}{2}(\nabla\phi)^2 - V(\phi)]. \tag{3.2.2}$$

Since the induced metric (3.1.3) depends only on τ, so ϕ also depends on τ. Thus Eq.(3.2.1) leads to

$$\rho = \frac{1}{2}[\dot{\phi}^2 + 2V(\phi)], \quad p = \frac{1}{2}[\dot{\phi}^2 - 2V(\phi)]. \tag{3.2.3}$$

In terms of scalar field, the integrated total energy density of the shell at some time is

$$m = 2\pi R^2[\dot{\phi}^2 + 2V(\phi)]. \tag{3.2.4}$$

Using Eqs.(3.2.3) and (3.2.4) in Eq.(3.1.12), we get

$$\ddot{\phi} + \frac{2\dot{R}}{R}\dot{\phi} + \frac{\partial V}{\partial\phi} = 0. \tag{3.2.5}$$

This is the Klien-Gordon (KG) equation, $\Box\phi + \frac{\partial V}{\partial\phi} = 0$, in coordinate system of the shell metric (3.1.3). In terms of scalar field, the effective potential is

$$\begin{aligned} V_{eff}(R) &= 1 - \left(\frac{M_+ - M_-}{2\pi R^2(\dot{\phi}^2 + 2V(\phi))}\right)^2 + \left(\frac{Q}{R}\right)^2 - \frac{(M_+ + M_-)}{R} \\ &- [\pi R(\dot{\phi}^2 + 2V(\phi))]^2. \end{aligned} \tag{3.2.6}$$

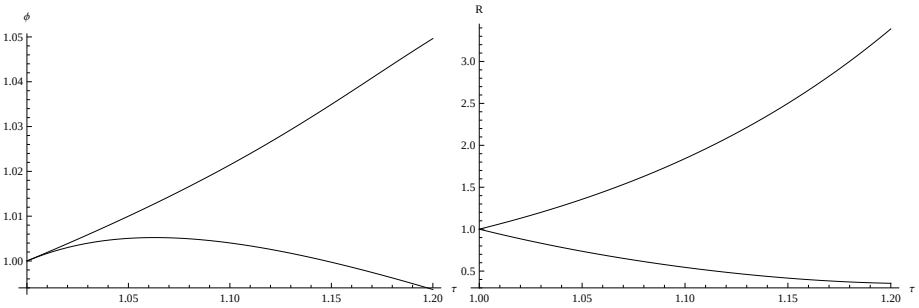

Figure 3.2: The left graph is the behavior of scalar field, while the right graph is the behavior of shell radius R. Both these graphs have been plotted by using $M_+ = 1,\ \tilde{m} = 1,\ M_- = 0,\ Q = 1,\ \dot{\phi}(1) = 0.19$ and $\phi(1) = R(1) = 1$.

Now we solve the KG equation (3.2.5) and equation of motion (3.1.15) (with Eq.(3.2.6)) simultaneously for $\phi(\tau)$ and $R(\tau)$. In this case, the exact solution is not possible. We solve these equations numerically by assuming the following initial conditions: $\dot{\phi}(1) = 0.19$ and $\phi(1) = R(1) = 1$. The solution of Eqs.(3.1.15) and (3.2.5) for the set of initial data are shown in Figure **3.2**. The left graph shows the behavior of scalar field in which upper and lower curves represent the expanding and collapsing shell, respectively. The right graph is the behavior of shell radius whose upper and lower curves represent the collapsing and expanding shell, respectively. In case of collapse (upper curve in left graph of Figure **3.2**), scalar field density ϕ goes on increasing while in case of expansion (lower curve in left graph of Figure **3.2**), scalar field density ϕ comes to a point on τ-axis implying that scalar field decays to zero value in this case. In the following, we shall explicitly discuss the massless and massive scalar field cases.

3.2.1 Massless Scalar Field

A scalar field becomes massless, when scalar potential, $V(\phi)$, is zero. In this case, the KG equation reduces to $\ddot{\phi}+\frac{2\dot{R}}{R}\dot{\phi}=0$ whose solution is $\dot{\phi}=\frac{\Omega}{R^2}$, where Ω is an integration constant. The corresponding equation of motion (3.1.15) with Eq.(3.2.6) takes the form

$$\dot{R}^2+1-\left(\frac{M_+-M_-}{2\pi\Omega^2}\right)^2R^4+\left(\frac{Q}{R}\right)^2-\frac{(M_++M_-)}{R}-\frac{\pi^2\Omega^4}{R^6}=0. \quad (3.2.7)$$

We define the following two parameters

$$[M]=M_+-M_-, \quad \overline{M}=\frac{M_++M_-}{2}.$$

Using these in Eq.(3.2.7), it follows that

$$\dot{R}^2+V_{eff}=0, \quad (3.2.8)$$

where

$$V_{eff}=1-\left(\frac{[M]}{2\pi\Omega^2}\right)^2R^4+\left(\frac{Q}{R}\right)^2-\frac{2\overline{M}}{R}-\frac{\pi^2\Omega^4}{R^6}. \quad (3.2.9)$$

For the initial data of shell, the left graph in Figure **3.3** shows the increase and decrease in shell radius implying the expansion and collapse of the massless scalar field shell. Thus a massless scalar shell may expand or collapse depending on the sign of velocity (i.e., $\dot{R}$) of the shell with respect to stationary observer. The behavior of the potential depends on the number of roots of the potential. If there is no root then the scalar field shell either expands indefinitely or collapses to zero size from some finite value. If there is one non-degenerate root then the shell expands to infinity or contracts to some finite size. For one degenerate root, the shell will be in an unstable equilibrium or collapses to form a BH or NS singularity.

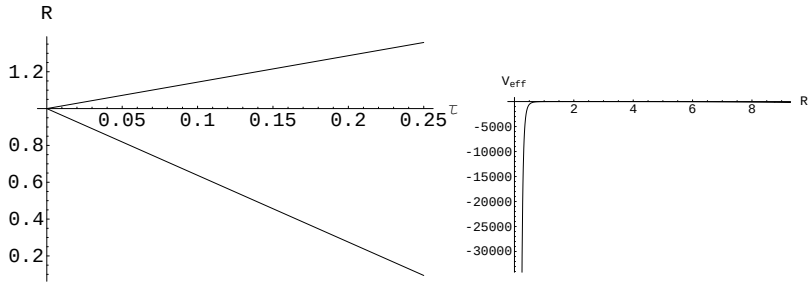

Figure 3.3: The left graph shows the shell radius for massless scalar field case. The right graph is the effective potential for massless scalar field with $\Omega = 1$, keeping all the remaining parameters and initial conditions same as in Figures 3.1, 3.2.

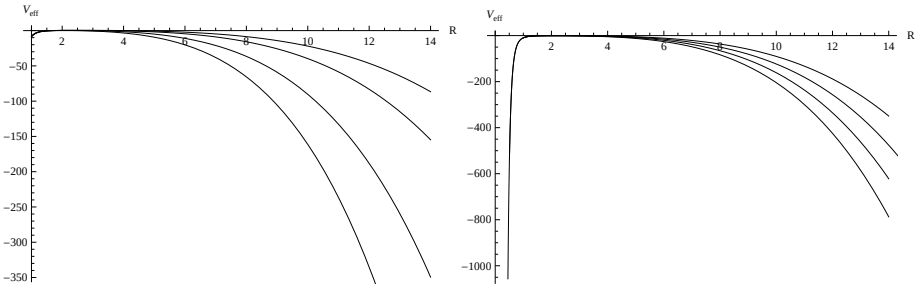

Figure 3.4: This describes the behavior of effective potential (Eq.(3.2.9)). Both graphs correspond to varying M_+ and M_-, keeping the remaining parameters same as in the previous cases.

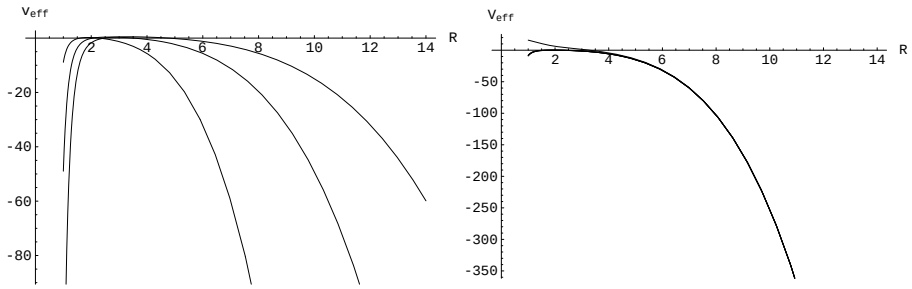

Figure 3.5: The left graph describes the effective potential for massless scalar field with different values of Ω, keeping all the remaining parameters same as in previous cases. The right graph represents the behavior of the massless scalar field shell for different values of the charge Q.

The graphical representation of the effective potential with same values of the parameters is shown in Figures **3.4, 3.5**. Both graphs for varying M_+ and M_- in Figure **3.4** and the left graph in Figure **3.5** show that the effective potential diverges for initial values of R and then $V_{eff} \to -\infty$ as $R \to \infty$. In these cases, the shell expands to infinity or collapses to zero size. The right graph in Figure **3.5** shows that the effective potential has one root and there occurs unstable situation, after which potential diverges negatively and the shell expands or collapses. The cases in which collapse occurs, the shell collapses to zero size by forming a curvature singularity at which intrinsic Ricci scalar of the shell, $R^{\mu}{}_{\mu} = -\frac{2}{R^2}(2R\ddot{R} + \dot{R}^2)$, diverges.

3.2.2 Massive Scalar Field

In this case, we discuss the motion of scalar field for which potential term, $V(\phi)$, is determined by taking p as an explicit function of R. From Eq.(3.2.3), we get

$$\dot{\phi}^2 = p + \rho, \quad V(\phi) = \frac{1}{2}(p - \rho). \tag{3.2.10}$$

Here we use p as an explicit function of R, [94] i.e., $p = p_0 e^{-kR}$, where p_0 and k are constants. Inserting this value of p in Eq.(3.1.11), we obtain

$$\rho = \frac{\chi}{R^2} + \frac{2(1+kR)p_0 e^{-kR}}{k^2 R^2}, \tag{3.2.11}$$

where χ is constant of integration. Notice that the above equations satisfy the conservation equation (3.1.11). Further, applying the values of p and ρ in Eq.(3.2.10), we get

$$V(\phi) = \frac{\chi}{2R^2} - \frac{p_0 e^{-kR}}{2}\left(1 - \frac{2(1+kR)}{k^2R^2}\right), \tag{3.2.12}$$

$$\dot{\phi}^2 = \frac{\chi}{R^2} + p_0 e^{-kR}\left(1 + \frac{2(1+kR)}{k^2R^2}\right). \tag{3.2.13}$$

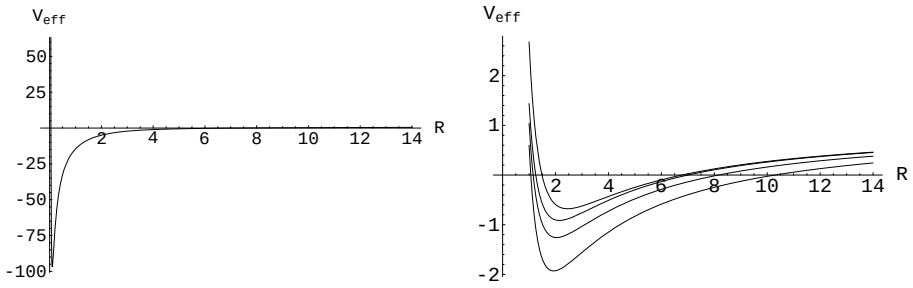

Figure 3.6: The behavior of effective potential for massive scalar field is shown for the fixed values of all parameters but varying charge parameter.

These equations satisfy the KG equation (3.2.5). Using Eqs.(3.2.11)-(3.2.13) in (3.2.6), we get

$$V_{eff}(R) = 1 - \left(\frac{M_+ - M_-}{m}\right)^2 + \left(\frac{Q}{R}\right)^2 - \frac{(M_+ + M_-)}{R} - \left(\frac{m}{2R}\right)^2, \quad (3.2.14)$$

where

$$m = 4\pi R^2 \rho \equiv 4\pi\chi + \frac{8\pi p_0 e^{-kR}}{k^2}(1 + kR). \quad (3.2.15)$$

The behavior of effective potential for massive scalar field shell is shown in Figure **3.6**. The left graph is effective potential for massive scalar field (Eq.(3.2.14)) when $k = 1,\ \chi = 3, p_0 = 1$, keeping the remaining parameters same as in the massless scalar field case. This implies that $V_{eff} \to -\infty$ as $R \to 0$, the massive shell collapses to zero size forming a curvature singularity. The right graph represents effective potential for massive scalar field shell with different values of Q.

There exist such values of charge parameter for which scalar field shell executes an oscillatory motion. The oscillations occur at two points where V_{eff} cuts the horizontal axis. The values of R for which $V_{eff} = 0$ are shown in the right graph of Figure **3.6** yielding zero velocity. This implies that the shell stops for a moment and then expands or collapses. During the collapsing phase at minimum values of the radius, the tangential pressure

reaches its maximum values while during the expansion, minimum pressure occurs at maximum radius. In this way, the scalar field shell performs the oscillatory motion. The values of R for which $V_{eff} = 0$, and intrinsic curvature of the shell is finite, are bouncing points, after bounce, the shell either expands or collapses.

3.3 Polytropic Matter Thin Shell Collapse

The equation of state for the polytropic matter is

$$p = k\rho^{(1+\frac{1}{n})}, \tag{3.3.1}$$

where k is EoS parameter and n denotes the polytropic index. Notice that different values of n correspond to different types of matter, for example, for $n \to \infty$, we have perfect fluid for which energy density is given by (3.1.13). The solution of Eq.(3.1.11), by using (3.3.1), for finite values of n is

$$\rho = \{(k + \rho_0{}^{\frac{-1}{n}})(\frac{R}{R_0})^{\frac{2}{n}} - k\}^{-n}, \tag{3.3.2}$$

where R_0 is the position of the shell at $\tau = \tau_0$ as mentioned earlier. We note that energy density for polytropic matter diverges at $R = R_0(\frac{k}{k+\rho_0{}^{\frac{-1}{n}}})^{\frac{n}{2}}$.

Using $x = \frac{R}{R_0}$, $t = \frac{\tau}{R_0}$ and Eq.(3.3.2) in Eqs.(3.1.15) and (3.1.16), we obtain equation of motion for polytropic matter with finite n

$$\dot{x}^2 + V_{eff}(x) = 0, \tag{3.3.3}$$

where

$$V_{eff}(x) = 1 - \frac{\varepsilon_+}{x} + \frac{\tilde{Q}^2}{x^2} - \frac{\varepsilon_-^2\zeta^2}{4x^4}(x^{\frac{2}{n}} - d)^{2n} - \frac{x^2}{\zeta^2(x^{\frac{2}{n}} - d)^{2n}}. \tag{3.3.4}$$

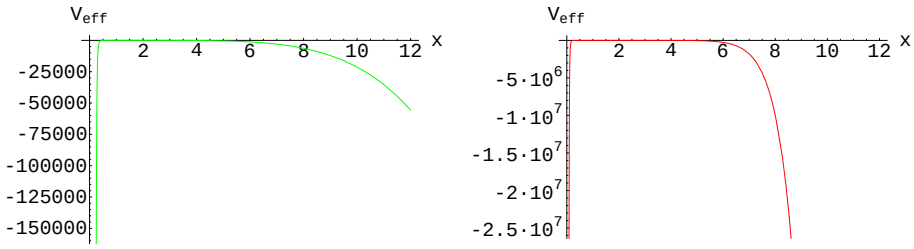

Figure 3.7: Both graphs represent the effective potential for the polytropic matter shell (3.3.4). The left graph corresponds to $n = 30$ and $k = 2$ while the right graph for $n = -30$ and $k = 2$. For both graphs, the values of the parameters are $M_- = 0, M_+ = R_0 = \rho_0 = Q = 1, \kappa = 8\pi$. These values of the parameters will remain the same for each graph while the extra parameters will be mentioned.

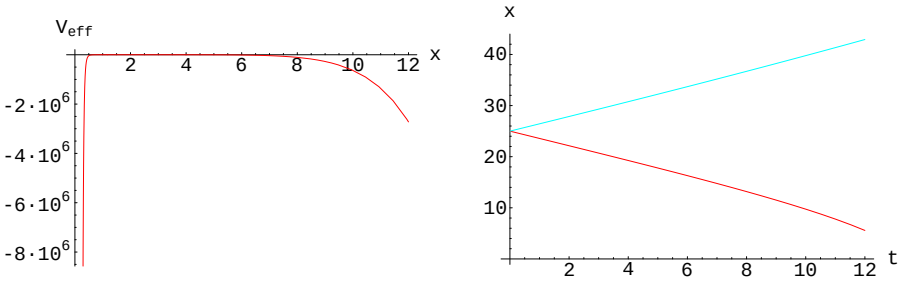

Figure 3.8: The left graph shows the effective potential for the perfect fluid shell (3.3.5) with $k = 2$. The right graph represents the increase and decrease in the shell radius with the increase of time for $x(0) = 25$.

Here $\varepsilon_\pm = \frac{(M_+ \pm M_-)}{R_0}$, $\tilde{Q} = \frac{Q}{R_0}$, $d = \frac{k}{k+\rho_0^{\frac{-1}{n}}}$, $\zeta = 4\frac{(k+\rho_0^{\frac{-1}{n}})^n}{\kappa R_0}$. Similarly, we use Eq.(3.1.14) in (3.1.16) and get the effective potential for infinite n (perfect fluid) case, given by

$$V_{eff}(x) = 1 - \frac{\varepsilon_+}{x} + \frac{\tilde{Q}^2}{x^2} - \frac{\bar{\zeta}^2}{x^{2+4k}} - \frac{\varepsilon_-^2 x^{4k}}{4\bar{\zeta}^2}, \tag{3.3.5}$$

where $\bar{\zeta} = \frac{1}{4}\kappa\rho_0 R_0{}^{(1-4k)}$.

Now we discuss Eqs.(3.3.3)-(3.3.5) graphically following the recent papers [181, 182]. Figure **3.7** describes the behavior of effective potential (3.3.4) for the collapsing polytropic matter with finite n and shell initial

data. The left graph in Figure **3.8** indicates the behavior of effective potential (3.3.5) for the perfect fluid shell depending on the EoS parameter and shell initial data. All these graphs show that $V_{eff} \leqslant 0$, thus Eq.(3.3.3) implies that motion is possible as $\dot{x}^2 \geqslant 0$. The left graphs in both figures show that the effective potential increases from $-\infty$ to 0 and then decreases from 0 to finite negative value. This implies that expanding or collapsing shell of matter comes to rest and then expands or collapses. The right graph in Figure **3.7** represents the following three phases.

1. Initially $V_{eff} \to -\infty$ as $x \to 0$, in this case, polytropic matter shell will expand to infinity for large initial radius or collapses to zero radius, forming a BH or NS. Bouncing would occur during the formation of BH and NS if initial shell velocity is negative and positive, respectively.

2. When $V_{eff} \to 0$ for $x > 0$, the matter shell attains the non-static equilibrium state as x increases.

3. $V_{eff} \to -\infty$ for some values of x. This implies that static shell comes to the state of expansion or collapse. In case of no crossing to x-axis, the shell collapses to zero or expands to infinity depending on the choice of the shell initial data.

Since the equation of motion (3.3.3) is nonlinear, its exact solution is impossible but can be solved numerically. The numerical solution of this equation for suitable choice of initial data and for some initial value of shell radius gives the behavior of the shell radius with respect to time shown in right graph of Figure **3.8**. This shows that radius is decreasing (increasing) function of time which is the strong argument for a shell to collapse

(expand).

3.3.1 Effects of NC Parameter on Polytropic Matter Thin Shell collapse

In this section, we study gravitational collapse in the NC RN geometry. The line element for NC RN metric is [98]

$$(ds)^2_{\pm} = N_{\pm}dT^2 - \frac{1}{N_{\pm}}dR^2 - R^2(d\theta^2 + \sin^2\theta d\phi^2), \tag{3.3.6}$$

where

$$\begin{aligned} N_{\pm}(R) &= 1 - \frac{4M_{\pm}}{R\sqrt{\pi}}\gamma\left(\frac{3}{2};\frac{R^2}{4\Theta}\right) + \frac{Q^2}{\pi R^2}\gamma^2\left(\frac{1}{2};\frac{R^2}{4\Theta}\right) - \frac{Q^2}{\pi R\sqrt{2\Theta}}\gamma\left(\frac{1}{2};\frac{R^2}{2\Theta}\right) \\ &+ \frac{Q^2}{\pi R}\sqrt{\frac{2}{\Theta}}\gamma(\frac{3}{2};\frac{R^2}{4\Theta}) \end{aligned}$$

and lower incomplete gamma function is defined by

$$\gamma\left(\frac{a}{b};x\right) = \int_0^x t^{\frac{a}{b}-1}e^{-t}dt. \tag{3.3.7}$$

In the commutative limit $\frac{R}{\sqrt{\Theta}} \longrightarrow \infty$, i.e., $\Theta \to 0$, Eq.(3.3.6) reduces to conventional RN metric (3.1.1). Here we assume smeared source in the NC geometry and use the modified energy density and pressure [102] $\rho_m = \rho_s + \rho_\Theta$ and $p_m = p_s + p_\perp$, respectively. The quantities ρ_s and p_s are the energy density and pressure of the shell used in the previous section, while ρ_Θ and $p_\perp$ are the energy density and pressure of the smeared source in NC theory.

It can be found [102] that ρ_Θ and $p_\perp$ satisfy the following relation

$$p_\perp = -(1 - \frac{R^2}{4\Theta})\rho_\Theta. \tag{3.3.8}$$

Hence, from Eq.(3.1.12), the NC energy density is $\rho_\Theta = \bar{\rho}e^{-(\frac{R^2-R_0^2}{4\Theta})}$, where $\bar{\rho}$ is the value of ρ_Θ at position R_0. It is interesting to note that when

$R \to 0$ or $\Theta \to \infty$, this matter acts as a matter of constant density. Thus the modified energy density for finite n is

$$\rho_m = \{(k+\rho_0{}^{\frac{-1}{n}})(\frac{R}{R_0})^{\frac{2}{n}} - k\}^{-n} + \bar{\rho}e^{-(\frac{R^2-R_0^2}{4\Theta})}. \tag{3.3.9}$$

Also, for perfect fluid, we have

$$\rho_m = \rho_0(\frac{R_0}{R})^{2k+2} + \bar{\rho}\ e^{-(\frac{R^2-R_0^2}{4\Theta})}. \tag{3.3.10}$$

The effective potential (3.1.16) in this case can be modified as follows

$$V_{eff}(R) = \frac{1}{2}(N_+ + N_-) - \frac{(N_+ - N_-)^2}{(\kappa\rho_m R)^2} - \frac{1}{16}(\kappa\rho_m R)^2. \tag{3.3.11}$$

Using $x = \frac{R}{R_0}$ and $t = \frac{\tau}{R_0}$ as in the previous case, we get the modified energy density and effective potential for finite n as follows

$$\rho_m = \{(k+\rho_0{}^{\frac{-1}{n}})x^{\frac{2}{n}} - k\}^{-n} + \bar{\rho}e^{-R_0^2(\frac{x^2-1}{4\Theta})}, \tag{3.3.12}$$

$$\begin{aligned} V_{eff}(x) &= 1 - \frac{\varepsilon_+}{x} + \frac{\tilde{Q}^2}{x^2} - \frac{4\varepsilon_-^2}{\kappa^2 R_0^2 x^4}\left(\{(k+\rho_0{}^{\frac{-1}{n}})x^{\frac{2}{n}} - k\}^{-n} + \bar{\rho}e^{-R_0^2(\frac{x^2-1}{4\Theta})}\right)^{-2} \\ &- \frac{R_0^2\kappa^2 x^2}{16}\left(\{(k+\rho_0{}^{\frac{-1}{n}})x^{\frac{2}{n}} - k\}^{-n} + \bar{\rho}e^{-R_0^2(\frac{x^2-1}{4\Theta})}\right)^2. \end{aligned} \tag{3.3.13}$$

The effective potential for the perfect fluid is

$$\begin{aligned} V_{eff}(x) &= 1 - \frac{\varepsilon_+}{x} + \frac{\tilde{Q}^2}{x^2} - \frac{4\varepsilon_-^2}{\kappa^2 R_0^2 x^4}\{\rho_0(\frac{1}{x})^{(2k+2)} + \bar{\rho}e^{-R_0^2(\frac{x^2-1}{4\Theta})}\}^{-2} \\ &- \frac{R_0^2\kappa^2 x^2}{16}\{\rho_0(\frac{1}{x})^{(2k+2)} + \bar{\rho}e^{-R_0^2(\frac{x^2-1}{4\Theta})}\}^2. \end{aligned} \tag{3.3.14}$$

Now we discuss the behavior of Eqs.(3.3.11)-(3.3.14) graphically. It follows from Figures **3.9-3.12** that the effective potential increases from negative to zero for polytropic matter with varying Θ and fixed k. The similar behavior of the effective potential (3.3.14) for the perfect fluid shell is shown in the left graph of Figure **3.13**. It is mentioned here that we have

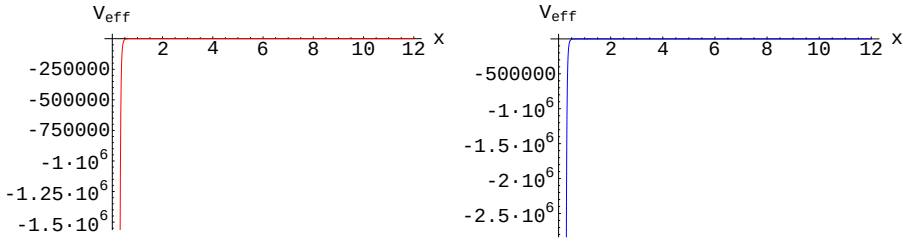

Figure 3.9: Both graphs show the effective potential for the polytropic matter shell in NC background (3.3.13). The left graph corresponds to $n = 30$ and $\Theta = 4$, while the right graph for $n = 30$ and $\Theta = 8$. For both graphs $k = 2,\ \bar{\rho} = 1$.

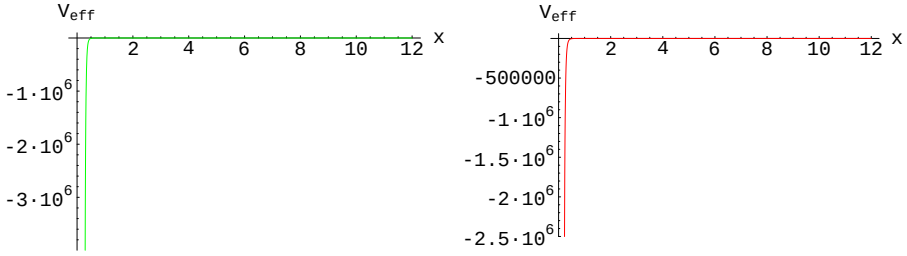

Figure 3.10: These indicate the effective potential for the polytropic matter shell in NC background (3.3.13). The left graph corresponds to $n = 30$ and $\Theta = 12$, while the right graph to $n = -30$ and $\Theta = 4$.

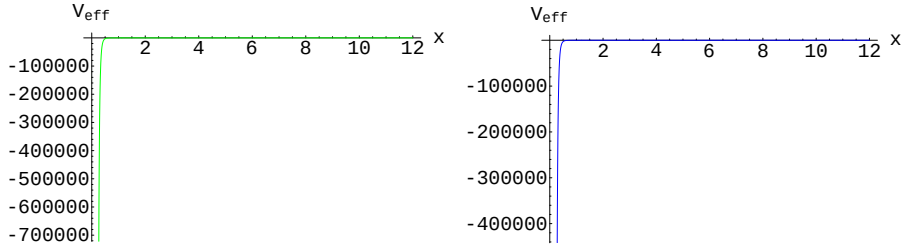

Figure 3.11: Both graphs represent the effective potential (3.3.13) corresponding to $n = -30,\ \Theta = 8$ and $\Theta = 12$.

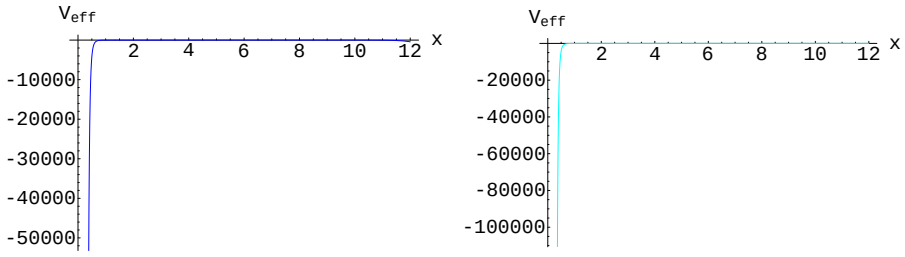

Figure 3.12: The effective potential (3.3.14) corresponding to $\Theta = 4$ and $\Theta = 8$ respectively.

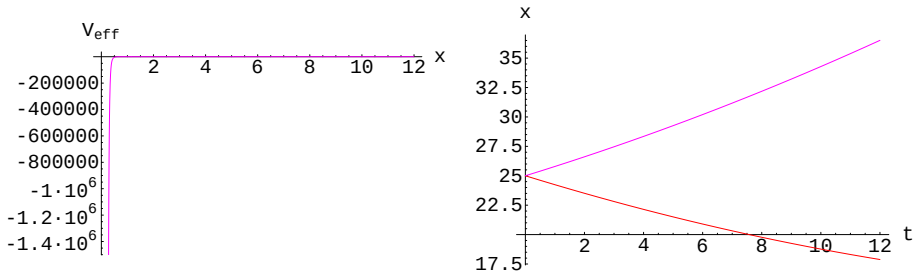

Figure 3.13: The effective potential of the perfect fluid shell corresponding to $\Theta = 12$ is shown in the left graph. The right graph shows that shell radius is increasing or decreasing function of t which corresponds to expansion or collapse.

only considered the case for which $k > 0$ in order to exclude the possibility of the exotic matter (DE) shell for which $k < 0$. This implies that depending on the choice of initial data, the shell continuously expands or collapses to a finite size then comes to rest position.

After a shell attains a last stage of rest position, it has no capability to re-expand or re-collapse to zero size. All the graphs in NC background have $V_{eff} \to -\infty$ at $x > 0$, neither of them is divergent at $x = 0$. This confirms that NC can measure short distances up to the order of Planck length scale. This can be seen by investigating the horizon radius and point of singularity where density diverges. The exact solution of nonlinear

equation of motion (3.3.3) with effective potentials in NC case is impossible. As before, we solve this equation by using numerical technique with initial condition. The behavior of the shell radius in this case is shown in right graph of Figure **3.13**.

The BH horizon can be found by solving

$$\begin{aligned} 1 \quad & -\frac{4M_{\pm}}{xR_0\sqrt{\pi}}\gamma\left(\frac{3}{2};\frac{(xR_0)^2}{4\Theta}\right)+\frac{Q^2}{\pi(xR_0)^2}\gamma^2\left(\frac{1}{2};\frac{(xR_0)^2}{4\Theta}\right)-\frac{Q^2}{\pi(xR_0)\sqrt{2\Theta}} \\ \times \quad & \gamma\left(\frac{1}{2};\frac{(xR_0)^2}{2\Theta}\right)+\frac{Q^2}{\pi(xR_0)}\sqrt{\frac{2}{\Theta}}\gamma\left(\frac{3}{2};\frac{(xR_0)^2}{4\Theta}\right)=0. \end{aligned} \tag{3.3.15}$$

For $R_0 = 1,\ Q = 1,\ M_+ = 1,\ M_- = 0$ and taking initially $x_h = 0.1$, the position of the horizon by iterative method is

$$\begin{aligned} x_h &= 1.35862; \qquad \Theta = 4, \\ x_h &= 1.70161; \qquad \Theta = 8, \\ x_h &= 1.94338; \qquad \Theta = 12. \end{aligned} \tag{3.3.16}$$

For finite n, the modified energy density (3.3.12) as well as the effective potential (3.3.13) for polytropic matter shell in NC case are singular at $x_s = \frac{k^{\frac{n}{2}}}{(k+\rho_0^{\frac{-1}{n}})^{\frac{n}{2}}}$. Although this is independent of Θ but it is the only value of x at which the modified energy density and effective potential diverge.

Further, all graphs of the effective potential for polytropic matter in Figures **3.9-3.12** for NC case imply that V_{eff} diverges negatively at $x > 0$, while the right graph of Figure **3.7** in commutative case for polytropic matter imply that $V_{eff} \to -\infty$ at $x = 0$. This means that the NC parameter Θ has shifted the singularity from $x = 0$ to $x > 0$. Hence, for the values of the parameters, $k,\ n$ and ρ_0 used for the solutions previously, we obtain $x_s = 0.00228365$ at which polytropic matter shell in NC case becomes singular. From the values of x_h and x_s, we conclude that "shell radii are

Figure 3.14: An artistic view of gravitational collapse in GR and NC theories of gravity. The shell before collapse is composed of matter, after collapse in GR matter is contracted to a point, while in NC approach matter is contracted within an inner small circle. According to GR, the shell collapses to zero radius leaving behind event horizon while in NC, it collapses to non-zero radius interior to the event horizon.

greater than the singular point (where density diverges)" i.e., horizon covers the singularity at point $x_s = 0.00228365$, which leads to the formation of BH as the final fate of the collapse as shown in Figure **3.14**.

For the case of infinite n, the energy density as well as effective potential diverge at $x = 0$. Thus for each value of Θ, the corresponding values of horizon radius are greater than zero, hence a singular shell of zero radius seems to be covered by the horizon radius. Consequently, we can say that perfect fluid shell collapse in NC geometry always ends as a BH. Hence in NC case, polytropic matter shell collapses to a small circle of non-zero radius, while perfect fluid shell collapses to zero radius. The clear effects of Θ appear in the presence of generic polytropic matter.

Chapter 4

Charged Perfect Fluid Collapse in Friedmann and 5D Tolman-Bondi Models

In this chapter, we discuss charged perfect fluid collapse in Friedmann and 5D TB models with positive cosmological constant. This provides an extension of perfect fluid collapse with positive cosmological constant [32, 72] to charged perfect fluid collapse with positive cosmological constant. The format of this chapter is the following. In section **4.1**, we explore charged perfect fluid collapse in Friedmann universe model. Using junction conditions between the Friedmann universe model and charged de-Sitter solution, we find analytic solution of the Einstein-Maxwell field equations. The formation of apparent horizons and their physical significance is discussed. Section **4.2** extends this procedure for charged perfect fluid collapse in 5D TB model. The contents of this chapter have been published in the form of two research papers [183, 184].

4.1 Charged Perfect Fluid Collapse in Friedmann Universe Model

This section is devoted to study the charged perfect fluid collapse in the Friedmann universe model. For this purpose, we discuss junction conditions, which help to explore solution of the field equations. Also, we find marginally bounded solution and investigate physical significance of apparent horizons.

4.1.1 Junction Conditions

Here, we formulate conditions for smooth matching of interior and exterior regions of a star on the boundary surface Σ. To this end, we assume that a spacelike 3D hypersurface divides two 4D manifolds M^- and M^+ as interior and exterior regions, respectively. The interior manifold is taken as Friedmann model [1]

$$ds^2_- = dt^2 - a(t)^2\left(d\chi^2 + f_k^2(d\theta^2 + \sin\theta^2 d\phi^2)\right), \tag{4.1.1}$$

where $f_k(\chi)$ can be defined as

$$f(\chi) = \begin{cases} \sin\chi, & k = 1 \\ \chi, & k = 0, \\ \sinh\chi, & k = -1, \end{cases}$$

$k = 1, 0, -1$ correspond to closed, flat and open universe models respectively, χ is the hyper-spherical angle such that $0 \leq \chi < \infty$ for open and flat models but $0 \leq \chi < 2\pi$ for closed model and $a(t)$ is the scale factor. Further, χ is related to radial coordinate r as follows

- $r = \sin\chi$ (closed)

- $r = \chi$ (flat)
- $r = \sinh\chi$ (open).

The RN de-Sitter spacetime is taken as exterior manifold

$$ds_+^2 = GdT^2 - \frac{1}{G}dR^2 - R^2(d\theta^2 + \sin\theta^2 d\phi^2), \tag{4.1.2}$$

where

$$G(R) = 1 - \frac{2m}{R} + \frac{Q^2}{R^2} - \frac{\Lambda}{3}R^2,$$

m and Λ are constants and Q is the charge. The equation of hypersurface in terms of interior spacetime M^- coordinates is

$$h_-(\chi, t) = \chi - \chi_\Sigma = 0, \tag{4.1.3}$$

where χ_Σ is a constant as Σ is a comoving surface forming the boundary of interior matter. Also, the equation of hypersurface in terms of exterior spacetime M^+ coordinates is given by

$$h_+(R, T) = R - R_\Sigma(T) = 0. \tag{4.1.4}$$

Using Eq.(4.1.3) in (4.1.1), the interior metric on Σ takes the form

$$(ds_-^2)_\Sigma = dt^2 - a(t)^2 f_k(\chi_\Sigma)(d\theta^2 + \sin\theta^2 d\phi^2). \tag{4.1.5}$$

Also, Eqs.(4.1.4) and (4.1.2) yield

$$(ds_+^2)_\Sigma = \left(G(R_\Sigma) - \frac{1}{G(R_\Sigma)}(\frac{dR_\Sigma}{dT})^2\right)dT^2 - R_\Sigma^2(d\theta^2 + \sin\theta^2 d\phi^2), \tag{4.1.6}$$

where we assume that

$$G(R_\Sigma) - \frac{1}{G(R_\Sigma)}(\frac{dR_\Sigma}{dT})^2 > 0,$$

so that T is a timelike coordinate. From Eqs.(1.16.1), (4.1.5) and (4.1.6), it follows that

$$R_\Sigma = (af_k)_\Sigma, \tag{4.1.7}$$

$$\left(G(R_\Sigma) - \frac{1}{G(R_\Sigma)}\left(\frac{dR_\Sigma}{dT}\right)^2\right)^{\frac{1}{2}} dT = dt. \tag{4.1.8}$$

Also, from (4.1.3)-(4.1.6), the outward unit normals (1.16.4) in terms of interior and exterior coordinates are given by

$$n_\mu^- = (0, a(t), 0, 0), \quad n_\mu^+ = (-\dot{R}_\Sigma, \dot{T}, 0, 0). \tag{4.1.9}$$

The components of the extrinsic curvature $K_{ij}^\pm$ from Eqs.(1.16.3) and (4.1.9) are

$$\begin{aligned} K_{00}^- &= 0, \quad K_{22}^- = \csc^2\theta K_{33}^- = (f_k {f_k}' a)_\Sigma, \\ K_{00}^+ &= (\dot{R}\ddot{T} - \dot{T}\ddot{R} - \frac{G}{2}\frac{dG}{dR}\dot{T}^3 + \frac{3}{2G}\frac{dG}{dR}\dot{T}\dot{R}^2)_\Sigma, \\ K_{22}^+ &= \csc^2\theta K_{33}^+ = (GR\dot{T})_\Sigma, \end{aligned} \tag{4.1.10}$$

where dot and prime mean differentiation with respect to t and χ, respectively. The continuity of the second fundamental form gives

$$K_{00}^+ = 0, \quad K_{22}^+ = K_{22}^-. \tag{4.1.11}$$

Using Eqs.(4.1.10) and (4.1.11) along with Eqs.(4.1.7) and (4.1.8), the final form of junction conditions become

$$(\dot{f_k}')_\Sigma = 0, \tag{4.1.12}$$

$$m = (\frac{af_k}{2} - \frac{\Lambda}{6}(af_k)^3 + \frac{Q^2}{2af_k} + \frac{a\dot{a}^2}{2}{f_k}^3 - \frac{a}{2}f_k{f_k}'^2)_\Sigma. \tag{4.1.13}$$

Equations (4.1.7), (4.1.8), (4.1.12) and (4.1.13) are the necessary conditions for the smooth matching of interior and exterior regions of a star over the boundary surface.

4.1.2 Solution of Einstein-Maxwell Field Equations

In this section, we solve the Einstein-Maxwell field equations with cosmological constant, perfect fluid and electromagnetic field in the Friedmann universe model. The Einstein-Maxwell field equations with cosmological constant are given by

$$G_{\mu\nu} - \Lambda g_{\mu\nu} = \kappa(T_{\mu\nu} + T^{(em)}_{\mu\nu}). \tag{4.1.14}$$

Using Eqs.(1.2.3) and (2.1.11) in (4.1.14), we obtain

$$R_{\mu\nu} = 8\pi[(\rho+p)u_\mu u_\nu + \frac{1}{2}(p-\rho)g_{\mu\nu} + T^{(em)}_{\mu\nu} - \frac{1}{2}g_{\mu\nu}T^{(em)}] - \Lambda g_{\mu\nu}. \tag{4.1.15}$$

In this case, $u_\mu = \delta^0_\mu$.

Now we solve Maxwell equations (1.2.9). For this purpose, we assume that in comoving coordinates system the charge is at rest, so that the magnetic field in the interior of a star will be zero. Thus we can choose four potential and four current as follows

$$\phi_\mu = (\phi(t,\chi), 0, 0, 0), \quad J^\mu = \sigma u^\mu, \tag{4.1.16}$$

where σ is the charge density. Using Eqs.(1.2.2) and (4.1.16), the only non-zero component of the field tensor is

$$F_{01} = -F_{10} = -\frac{\partial\phi}{\partial\chi}. \tag{4.1.17}$$

Also, from Eqs.(1.2.9), (4.1.16) and (4.1.17), we have

$$\frac{1}{a^2}\left(\frac{\partial^2\phi}{\partial\chi^2} + 2\frac{{f_k}'}{f_k}\frac{\partial\phi}{\partial\chi}\right) = 4\pi\sigma, \tag{4.1.18}$$

$$\frac{\partial^2\phi}{\partial\chi\partial t} + \frac{\dot{a}}{a}\frac{\partial\phi}{\partial\chi} = 0. \tag{4.1.19}$$

Integration of Eq.(4.1.18) implies that

$$\frac{\partial\phi}{\partial\chi} = \frac{q}{a{f_k}^2}, \tag{4.1.20}$$

where $q(\chi) = 4\pi \int_0^\chi \sigma a^3 {f_k}^2 d\chi$ is the total amount of charge in the interior region of a star. This amount of charge can be obtained by the conservation law of charge, i.e., $J^\mu_{;\mu} = 0$. Notice that Eq.(4.1.19) is identically satisfied by Eq.(4.1.20).

The electromagnetic field intensity is given by

$$E = \frac{q}{(af_k)^2}. \tag{4.1.21}$$

where $E = 4\pi\tilde{E}$. Equations (4.1.20) and (4.1.21) yield

$$\frac{\partial\phi}{\partial\chi} = aE. \tag{4.1.22}$$

Using Eqs.(4.1.17) and (4.1.22), we obtain

$$F_{01} = -F_{10} = -aE. \tag{4.1.23}$$

The non-zero components of $T^{(em)}_{\mu\nu}$ and its trace turn out to be

$$\begin{aligned} T^{(em)}_{00} &= \frac{1}{8\pi}E^2, \quad T^{(em)}_{11} = -\frac{1}{8\pi}E^2a^2, \quad T^{(em)}_{22} = \frac{1}{8\pi}E^2(af_k)^2, \\ T^{(em)}_{33} &= T^{(em)}_{22}\sin^2\theta, \quad T^{(em)} = 0. \end{aligned}$$

Using these values, the Einstein-Maxwell field equations (4.1.15) for the interior spacetime take the following form

$$R_{00} = -3\frac{\ddot{a}}{a} = 4\pi(\rho + 3p) + E^2 - \Lambda, \tag{4.1.24}$$

$$R_{11} = -\frac{\ddot{a}}{a} - 2\left(\frac{\dot{a}}{a}\right)^2 + \frac{2}{a^2}\frac{{f_k}''}{f_k} = 4\pi(p - \rho) + E^2 - \Lambda, \tag{4.1.25}$$

$$\begin{aligned} R_{22} &= -\frac{\ddot{a}}{a} - 2\left(\frac{\dot{a}}{a}\right)^2 + \frac{1}{a^2}\left(\frac{{f_k}''}{f_k} + (\frac{{f_k}'}{f_k})^2 - \frac{1}{{f_k}^2}\right) \\ &= 4\pi(p - \rho) - E^2 - \Lambda, \end{aligned} \tag{4.1.26}$$

$$R_{33} = \sin^2\theta R_{22}, \tag{4.1.27}$$

When we talk about a field then there is a force associated with this field which acts on the underlying geometry and causes the distortion. The electromagnetic force associated with electromagnetic field in the Friedmann

universe model causes to disturb the generic properties of the Friedmann universe model. In order to preserve the homogeneity and isotropy of the model, we assume that matter field is much stronger than the electromagnetic field [120], i.e., $E^2 << \rho$. Thus all the results are valid for $E^2 << \rho$ and hence for stiff matter (i.e., $\rho = p$), $E^2 << p$. Integrating Eq.(4.1.12) with respect to t, it follows that

$$f_k{}' = w,$$

where $w = w(\chi)$ is an arbitrary function of χ.

The energy conservation equation, $T^{\nu}_{\mu;\nu} = 0$, for perfect fluid with interior metric shows that pressure is a function of t only, i.e.,

$$p = p(t).$$

Using these values of $f_k{}'$ and p in Eqs.(4.1.24)-(4.1.27), it follows that

$$2\frac{\ddot{a}}{a} + \left(\frac{\dot{a}}{a}\right)^2 + \frac{(1-w^2)}{(af_k)^2} = \Lambda + E^2 - 8\pi p(t). \tag{4.1.28}$$

We consider p as a polynomial in t as given by [32]

$$p(t) = p_0(\frac{t}{T})^{-c}, \tag{4.1.29}$$

where T is the constant time introduced in the problem due to physical reason by re-scaling of t, p_0 and c are positive constants. Further, for simplicity, we take $c = 0$ so that

$$p(t) = p_0.$$

Equation (4.1.28) gives

$$2\frac{\ddot{a}f_k}{af_k} + \left(\frac{\dot{a}f_k}{af_k}\right)^2 + \frac{(1-w^2)}{(af_k)^2} = \Lambda + E^2 - 8\pi p_0. \tag{4.1.30}$$

Since in comoving coordinates system the charge is at rest, so E is taken as time independent [185]. Integration of the above equation with respect to t yields

$$(\dot{a}f_k)^2 = w^2 - 1 + (\Lambda + E^2 - 8\pi p_0)\frac{a^2 {f_k}^2}{3} + 2\frac{M}{(af_k)^2}, \tag{4.1.31}$$

where $M = M(\chi)$ is an arbitrary function of χ which is related to the mass of the collapsing system. Substituting the values of ${f_k}'$ and $\dot{a}f_k$ in Eq.(4.1.24), we get

$$M' = \frac{2E'E}{3}(af_k)^3 + a^3 {f_k}' {f_k}^2 (4\pi\left(p_0 + \rho\right) + 2E^2)\,. \tag{4.1.32}$$

For physical reasons, we assume that $(p_0+\rho) \geqslant 0$. Integrating this equation with respect to χ, we obtain

$$M(\chi) = 4\pi a^3 \int_0^\chi (\rho+p_0){f_k}' {f_k}^2 d\chi + 2\int_0^\chi E^2 {f_k}' {f_k}^2 d\chi + \frac{2}{3}a^3 \int_0^\chi E'E {f_k}^3 d\chi + M_0, \tag{4.1.33}$$

where M_0 is integration constant which can be taken to be zero due to finite distribution of matter at the center of spherical symmetry.

The function $M(\chi)$ should be positive, otherwise $M(\chi) < 0$ implies that mass is non-physical. Using the values of ${f_k}'$ and $\dot{a}f_k$, into the junction condition (4.1.13), it follows that

$$m = \frac{M(\chi)}{af_k} + \frac{Q^2}{2af_k}. \tag{4.1.34}$$

Using Misner-Sharp definition of mass function [20], the total energy $\tilde{m}(\chi, t)$ inside the boundary surface Σ with the contribution of electromagnetic field and cosmological constant for the Friedmann model

$$\tilde{m}(\chi, t) = \frac{1}{2}(af_k)\left(1 - (\dot{a}f_k)^2 + {f_k}'^2\right) + \frac{q^2}{2af_k} - \frac{\Lambda}{6}(af_k)^3. \tag{4.1.35}$$

Replacing the values of ${f_k}'$ and $\dot{a}f_k$, we obtain

$$\tilde{m}(\chi,t)=\frac{M(\chi)}{af_k}+\frac{q^2}{2af_k}. \tag{4.1.36}$$

From Eqs.(4.1.34) and (4.1.36), it can be found that $\tilde{m}(\chi,t)=^{\Sigma} m$ if and only if $q=Q$. This result provides the necessary and sufficient conditions for the continuity of gravitational masses in the interior and exterior regions over the boundary surface Σ.

Now we take $(\Lambda+E^2-8\pi p_0)>0$ and assume that for marginally bounded solution $w(\chi)=1$. In order to obtain analytic solutions in closed form, we use Eqs.(4.1.2), (4.1.31) and $w(\chi)=1$ so that

$$af_k=(\frac{6m}{\Lambda+E^2-8\pi p_0})^{\frac{1}{3}}\sinh^{\frac{2}{3}}\alpha(\chi,t) \tag{4.1.37}$$

where

$$\alpha(\chi,t)=\frac{\sqrt{3(\Lambda+E^2-8\pi p_0)}}{2}(t_s-t).$$

Here, $t_s(\chi)$ is an integration function which is related to the time of formation of singularity. The time $t=t_s$ corresponds to the shell focusing singularity at $af_k=0$, where matter shell hit the physical singularity.

4.1.3 Apparent Horizons

Now we discuss the physical significance of apparent horizons, i.e., area of apparent horizons, time difference between the formation of apparent horizons and singularity etc. In 4D, an apparent horizon occurs when the boundary of trapped two spheres is formed. For the interior spacetime, we find this boundary of trapped two spheres whose outward normals are null as follows

$$g^{\mu\nu}(af_k)_{,\mu}(af_k)_{,\nu}=(\dot{a}f_k)^2-({f_k}')^2=0. \tag{4.1.38}$$

Using the values of ${f_k}'$ and $\dot{a}f_k$ in the above equation, it follows that

$$(\Lambda + E^2 - 8\pi p_0)(af_k)^3 - 3(af_k) + 6M = 0. \tag{4.1.39}$$

When $\Lambda = 8\pi p_0 - E^2$, we have $af_k = 2M$. This is called Schwarzschild horizon. For $M = p_0 = E = 0$, we have $af_k = \sqrt{\frac{3}{\Lambda}}$, which is called de-Sitter horizon.

Equation (4.1.39) can have the following positive roots.

Case (i): For $3M < \frac{1}{\sqrt{(\Lambda+E^2-8\pi p_0)}}$, we obtain two horizons

$$(af_k)_{ch} = \frac{2}{\sqrt{(\Lambda + E^2 - 8\pi p_0)}} \cos\frac{\varphi}{3}, \tag{4.1.40}$$

$$(af)_{bh} = \frac{-1}{\sqrt{(\Lambda + 8\pi E^2 - p_0)}}(\cos\frac{\varphi}{3} - \sqrt{3}\sin\frac{\varphi}{3}), \tag{4.1.41}$$

where

$$\cos\varphi = -3M\sqrt{(\Lambda + E^2 - 8\pi p_0)}. \tag{4.1.42}$$

If we take $M = 0$, it follows from Eqs.(4.1.40) and (4.1.41) that $(af_k)_{ch} = \sqrt{\frac{3}{(\Lambda+E^2-8\pi p_0)}}$ and $(af_k)_{bh} = 0$, where $(af_k)_{ch}$ and $(af_k)_{bh}$ are called cosmological and BH horizons, respectively.

Case (ii): For $3M = \frac{1}{\sqrt{(\Lambda+E^2-8\pi p_0)}}$, there is only one positive root which corresponds to a single horizon, i.e.,

$$(af_k)_{ch} = (af_k)_{bh} = \frac{1}{\sqrt{(\Lambda + E^2 - 8\pi p_0)}} = (af_k). \tag{4.1.43}$$

This shows that both horizons coincide. The range for the cosmological and BH horizons can be written as follows

$$0 \leq (af_k)_{bh} \leq \frac{1}{\sqrt{(\Lambda + E^2 - 8\pi p_0)}} \leq (af_k)_{ch} \leq \sqrt{\frac{3}{(\Lambda + E^2 - 8\pi p_0)}}. \tag{4.1.44}$$

The BH horizon has its largest proper area $4\pi(af_k)^2 = \frac{4\pi}{(\Lambda+E^2-8\pi p_0)}$ and cosmological horizon has its area between $\frac{4\pi}{(\Lambda+E^2-8\pi p_0)}$ and $\frac{12\pi}{(\Lambda+E^2-8\pi p_0)}$.

Case (iii): For $3M > \frac{1}{\sqrt{(\Lambda+E^2-8\pi p_0)}}$, there are no positive roots and consequently there is no apparent horizon.

We now calculate the time of formation of the apparent horizon by using Eqs.(4.1.37) and (4.1.39)

$$t_N = t_s - \frac{2}{\sqrt{3(\Lambda+E^2-8\pi p_0)}}\sinh^{-1}(\frac{(af_k)_N}{2M}-1)^{\frac{1}{2}}, \quad (N=1,2). \tag{4.1.45}$$

This implies that

$$\frac{(af_k)_N}{2M} = \cosh^2\alpha_N, \tag{4.1.46}$$

where $\alpha_N(r,\chi) = \frac{\sqrt{3(\Lambda+E^2-8\pi p_0)}}{2}[t_s(\chi)-t_N)]$, t_1, t_2 and t_s correspond to time formation of cosmological horizon, BH horizon and singularity. Equations (4.1.44) and (4.1.45) give $(af_k)_{ch} \geq (af_k)_{bh}$ and $t_{bh} \geq t_{ch}$, respectively. The inequality $t_{bh} \geq t_{ch}$ indicates that the cosmological horizon forms earlier than BH horizon. In general, Eq.(4.1.45) shows that $t_N \leq t_s$, which confirms the formation of BH.

The time difference between the formation of cosmological horizon and singularity and the formation of BH horizon and singularity can be found as follows. Using Eqs.(4.1.40)-(4.1.5), we have

$$\frac{d(\frac{(af_k)_{ch}}{2M})}{dM} = \frac{1}{M}(-\frac{\sin\frac{\varphi}{3}}{\sin\varphi}+\frac{3\cos\frac{\varphi}{3}}{\cos\varphi}) < 0, \tag{4.1.47}$$

$$\frac{d(\frac{(af_k)_{bh}}{2M})}{dM} = \frac{1}{M}(-\frac{\sin\frac{(\varphi+4\pi)}{3}}{\sin\varphi}+\frac{3\cos\frac{(\varphi+4\pi)}{3}}{\cos\varphi}) > 0. \tag{4.1.48}$$

The time difference between the formation of singularity and apparent horizons is

$$\tau_N = t_s - t_N. \tag{4.1.49}$$

It follows from Eq.(4.1.46) that

$$\frac{d\tau_N}{d(\frac{(af_k)_N}{2M})} = \frac{1}{\sinh\alpha_N\cosh\alpha_N\sqrt{3(\Lambda+E^2-8\pi p_0)}}. \tag{4.1.50}$$

Using Eqs.(4.1.47) and (4.1.50), we obtain

$$\frac{d\tau_1}{dM} = \frac{d\tau_1}{d(\frac{(af_k)_{ch}}{2M})}\frac{d(\frac{(af_k)_{ch}}{2M})}{dM} = \frac{1}{M\sqrt{3(\Lambda+E^2-8\pi p_0)}\sinh\alpha_1\cosh\alpha_1} \times (-\frac{\sin\frac{\varphi}{3}}{\sin\varphi}+\frac{3\cos\frac{\varphi}{3}}{\cos\varphi}) < 0. \quad (4.1.51)$$

Similarly, from Eqs.(4.1.49) and (4.1.50), we get

$$\frac{d\tau_2}{dM} = \frac{1}{M\sqrt{3(\Lambda+E^2-8\pi p_0)}\sinh\alpha_2\cosh\alpha_2} \times(-\frac{\sin\frac{(\varphi+4\pi)}{3}}{\sin\varphi}+\frac{3\cos\frac{(\varphi+4\pi)}{3}}{\cos\varphi}) > 0. \quad (4.1.52)$$

Equations (4.1.51) and (4.1.52) imply that the time interval between the formation of cosmological horizon (BH horizon) and singularity is decreasing (increasing) with the increase of mass.

4.2 Charged Perfect Fluid Collapse in 5D Tolman-Bondi Model

In this section, we investigate the charged perfect fluid collapse in 5D TB model. We discuss the matching conditions for 5D TB model and 5D RN de-Sitter solution. The analytic solution of the Einstein-Maxwell field equations with cosmological constant is found in 5D TB model. The formation of apparent horizons is also discussed.

4.2.1 Junction Conditions

A spacelike 4D hypersurface Σ is taken such that it divides a 5D spacetime into two 5D manifolds, M^- and M^+, respectively. The 5D TB spacetime is taken as an interior manifold M^- [69]

$$ds^2_- = dt^2 - X^2dr^2 - Y^2(d\theta^2+\sin^2\theta d\phi^2+\sin^2\theta\sin^2\phi d\psi^2), \quad (4.2.1)$$

where X and Y are functions of t and r. For the exterior manifold M^+, we take the 5D RN de-Sitter spacetime [186]

$$ds_+^2 = CdT^2 - \frac{1}{C}dR^2 - R^2(d\theta^2 + \sin^2\theta d\phi^2 + \sin^2\theta \sin^2\phi d\psi^2), \quad (4.2.2)$$

where

$$C(R) = 1 - \frac{2m}{R^2} + \frac{Q^2}{R^4} - \frac{\Lambda}{6}R^2,$$

m and Λ are constants and Q is the charge.

The equations of the hypersurface Σ in terms of the interior and exterior spacetimes are given as

$$k_-(r,t) = r - r_\Sigma = 0, \quad k_+(R,T) = R - R_\Sigma(T) = 0, \quad (4.2.3)$$

where r_Σ is a constant. Using Eq.(4.2.3) in (4.2.1) and (4.2.2), we obtain the following form of the interior and exterior spacetimes on the boundary surface Σ

$$(ds_-^2)_\Sigma = dt^2 - [Y(r_\Sigma,t)]^2(d\theta^2 + \sin^2\theta d\phi^2 + \sin^2\theta \sin^2\phi d\psi^2), \quad (4.2.4)$$

$$\begin{aligned}(ds_+^2)_\Sigma &= [C(R_\Sigma) - \frac{1}{C(R_\Sigma)}(\frac{dR_\Sigma}{dT})^2]dT^2 \\ &- R_\Sigma{}^2(d\theta^2 + \sin^2\theta d\phi^2 + \sin^2\theta \sin^2\phi d\psi^2). \quad (4.2.5)\end{aligned}$$

For T to be a timelike coordinate, we assume that

$$C(R_\Sigma) - \frac{1}{C(R_\Sigma)}(\frac{dR_\Sigma}{dT})^2 > 0.$$

From Eqs.(1.16.1), (4.2.4) and (4.2.5), it follows that

$$R_\Sigma = Y(r_\Sigma, t), \quad (4.2.6)$$

$$\left(C(R_\Sigma) - \frac{1}{C(R_\Sigma)}(\frac{dR_\Sigma}{dT})^2\right)^{\frac{1}{2}} dT = dt. \quad (4.2.7)$$

The outward unit normals to Σ in the coordinates of M^- and M^+ are

$$n_\mu^- = (0, X(r_\Sigma,t), 0, 0, 0), \quad n_\mu^+ = (-\dot{R}_\Sigma, \dot{T}, 0, 0, 0). \quad (4.2.8)$$

The components of the second fundamental form turn out to be

$$\begin{aligned} K^{-}_{00} &= 0, \quad K^{-}_{22} = \csc^2\theta K^{-}_{33} = \csc^2\theta\csc^2\phi K^{-}_{44} = \left(\frac{YY'}{X}\right)_{\Sigma}, \\ K^{+}_{00} &= \left(\dot{R}\ddot{T} - \dot{T}\ddot{R} - \frac{C}{2}\frac{dC}{dR}\dot{T}^3 + \frac{3}{2C}\frac{dC}{dR}\dot{T}\dot{R}^2\right)_{\Sigma}, \\ K^{+}_{22} &= \csc^2\theta K^{+}_{33} = \csc^2\theta\csc^2\phi K^{+}_{44} = \left(CR\dot{T}\right)_{\Sigma}, \end{aligned} \tag{4.2.9}$$

where dot and prime indicate differentiations with respect to t and r, respectively. The continuity of the second fundamental form gives

$$K^{+}_{00} = 0, \quad K^{+}_{22} = K^{-}_{22}. \tag{4.2.10}$$

When we make use of Eqs.(4.2.9) and (4.2.10) along with Eqs.(4.2.6) and (4.2.7), the junction conditions become

$$\left(X\dot{Y}' - \dot{X}Y'\right)_{\Sigma} = 0, \tag{4.2.11}$$

$$m = \left(\frac{Y^2}{2} + \frac{Q^2}{2Y^2} - \frac{\Lambda}{12}Y^4 + \frac{(\dot{Y}Y)^2}{2} - \left(\frac{YY'}{X}\right)^2\right)_{\Sigma}. \tag{4.2.12}$$

Equations (4.2.6), (4.2.7) and Eqs.(4.2.11), (4.2.12) are necessary conditions for the smooth matching of interior and exterior regions of a star.

4.2.2 Solution of Einstein-Maxwell Field Equations

We solve the Einstein-Maxwell field equations with positive cosmological constant in 5D TB model. We assume that the charged perfect fluid is in comoving coordinates system so that the magnetic field is zero. Consequently, the five potential and the five current can be taken as

$$\phi_{\mu} = (\phi(t,r), 0, 0, 0, 0), \quad J^{\mu} = \sigma\delta^{\mu}_{0}, \tag{4.2.13}$$

where σ is the charge density. In this case, the non-zero component of the field tensor is

$$F_{tr} = -F_{rt} = -\frac{\partial\phi}{\partial r}. \tag{4.2.14}$$

Also, Eqs.(1.2.9), (4.2.13) and (4.2.14) yield

$$\frac{\partial^2\phi}{\partial r^2}+\frac{\partial\phi}{\partial r}[\frac{3Y'}{Y}-\frac{X'}{X}] = 4\pi\sigma X^2, \tag{4.2.15}$$

$$\frac{\partial^2\phi}{\partial r\partial t}-\frac{\partial\phi}{\partial r}[\frac{\dot{X}}{X}+\frac{3\dot{Y}}{Y}] = 0. \tag{4.2.16}$$

Integration of Eq.(4.2.15) leads to

$$\frac{\partial\phi}{\partial r}=\frac{X}{Y^3}q, \tag{4.2.17}$$

where $q(r)=4\pi\int_0^r\sigma Y^3Xdr$ is the total amount of charge. By using Eqs. (4.2.14) and (4.2.17), we get

$$F_{tr}=-F_{rt}=-\frac{X}{Y^3}q. \tag{4.2.18}$$

The electromagnetic field intensity is

$$E=\frac{q}{Y^3}, \tag{4.2.19}$$

where $E=2\pi^2\tilde{E}$. Equations (4.2.18) and (4.2.19) yield

$$F_{tr}=-F_{rt}=-XE. \tag{4.2.20}$$

The non-zero components of $T_\mu^{\nu(em)}$ are

$$T_0^{0(em)}=T_1^{1(em)}=-T_2^{2(em)}=-T_3^{3(em)}=-T_4^{4(em)}=\frac{1}{8\pi}E^2.$$

Thus the Einstein-Maxwell field equations for the interior spacetime (4.2.1) with positive cosmological constant and perfect fluid are written as

$$G_0^0 = -\frac{3}{X^2}\left(\frac{Y''}{Y}-\frac{X'}{X}\frac{Y'}{Y}+\frac{Y'^2}{Y^2}\right)+3\left(\frac{\dot{Y}^2}{Y^2}+\frac{\dot{X}}{X}\frac{\dot{Y}}{Y}\right)+\frac{3}{Y^2}$$
$$= \Lambda+E^2+8\pi\rho, \tag{4.2.21}$$

$$G_1^1 = -\frac{3Y'^2}{X^2Y^2}+3\left(\frac{\ddot{Y}}{Y}+\frac{\dot{Y}^2}{Y^2}\right)+\frac{3}{Y^2}=\Lambda-8\pi p+E^2, \tag{4.2.22}$$

$$G_2^2 = -\frac{2}{X^2}\left(\frac{Y''}{Y} - \frac{X'}{X}\frac{Y'}{Y} - \frac{Y'^2}{2Y^2}\right) + 2\left(\frac{\ddot{Y}}{Y} + \frac{\dot{X}}{X}\frac{\dot{Y}}{Y} + \frac{\dot{Y}^2}{2Y^2} + \frac{\ddot{X}}{2X}\right)$$
$$+ \frac{1}{Y^2} = \Lambda - 8\pi p - E^2, \tag{4.2.23}$$
$$G_3^3 = G_4^4 = G_2^2 = \Lambda - 8\pi p - E^2, \tag{4.2.24}$$
$$G_1^0 = -3\left(\frac{\dot{Y}'}{Y} - \frac{\dot{X}}{X}\frac{Y'}{Y}\right) = 0. \tag{4.2.25}$$

To solve these equations, we integrate Eq.(4.2.25) with respect to t so that

$$X = \frac{Y'}{f}, \tag{4.2.26}$$

where $f = f(r)$ represents the energy inside the hypersurface Σ. Making use of Eqs.(4.2.22) and (4.2.26), it follows that

$$\frac{\ddot{Y}}{Y} + \left(\frac{\dot{Y}}{Y}\right)^2 + \frac{1-f^2}{Y^2} = \frac{1}{3}\left(\Lambda - 8\pi p + E^2\right) \tag{4.2.27}$$

The energy-momentum conservation equation for matter implies that $p = p(t)$. Using this value of p in the above equation, we obtain

$$\frac{\ddot{Y}}{Y} + \left(\frac{\dot{Y}}{Y}\right)^2 + \frac{1-f^2}{Y^2} = \frac{1}{3}\left(\Lambda - 8\pi p(t) + E^2\right). \tag{4.2.28}$$

We assume p to be in the form given by Eq.(4.1.29). Inserting this value of $p(t)$ in Eq. (4.2.28), we get

$$\frac{\ddot{Y}}{Y} + \left(\frac{\dot{Y}}{Y}\right)^2 + \frac{1-f^2}{Y^2} = \frac{1}{3}\left(\Lambda - 8\pi p_0 + E^2\right). \tag{4.2.29}$$

Also, integrating the above equation with respect to t, we have

$$\dot{Y}^2 = f^2 - 1 + \frac{2M}{Y^2} + (\Lambda - 8\pi p_0 + E^2)\frac{Y^2}{6}, \tag{4.2.30}$$

where M is an arbitrary function of r and is related to the mass of the collapsing system. Using Eqs.(4.2.26) and (4.2.30) in Eq.(4.2.21), we obtain

$$M' = \frac{8\pi}{3}(\rho + p_0)Y^3Y' - \frac{EE'}{6}Y^4. \tag{4.2.31}$$

We assume that ρ and p_0 satisfy the weak energy condition [1]

$$\rho \geq 0, \quad \rho + p_0 \geq 0. \tag{4.2.32}$$

Integrating Eq.(4.2.31) with respect to r, it follows that

$$M(r) = \frac{8\pi}{3}\int_0^r (\rho + p_0)Y^3Y' - \frac{1}{6}\int_0^r EE'Y^4, \tag{4.2.33}$$

where we have taken $M_0 = 0$ due to finite distribution of mass at $r = 0$.

The total energy $\tilde{m}(r,t)$ up to radius r at time t inside the hypersurface can be evaluated by using the definition of Misner-Sharp mass. For the interior metric with cosmological constant and electromagnetic field, it takes the form

$$\tilde{m}(r,t) = \left(\frac{Y^2}{2} + \frac{q^2}{2Y^2} - \frac{\Lambda}{12}Y^4 + \frac{(\dot{Y}Y)^2}{2} - \left(\frac{YY'}{X}\right)^2\right)_{\Sigma}. \tag{4.2.34}$$

Comparing the above equation with (4.2.12), we get $\tilde{m}(r,t) =^{\Sigma} m$ if and only if $q = Q$. This shows the continuity of gravitational masses in both regions over boundary surface.

Now we solve Eq.(4.2.30) for the following two cases:

$$f(r) = 1, \quad f(r) \neq 1.$$

Case A: Solution with $f(r) = 1$

For $\Lambda - 8\pi p_0 + E^2 > 0$, the analytic solutions in closed form can be obtained from Eqs.(4.2.26) and (4.2.30) as follows

$$Y(r,t) = \left(\frac{12M}{\Lambda - 8\pi p_0 + E^2}\right)^{\frac{1}{4}} \sinh^{\frac{1}{2}} \alpha(r,t), \tag{4.2.35}$$

$$
\begin{aligned}
X(r,t) &= \left(\frac{12M}{\Lambda+E^2-8\pi p_0}\right)^{\frac{1}{4}}\left[\left(\frac{4M'}{M}-\frac{2EE'}{\sqrt{(\Lambda+E^2-8\pi p_0)}}\right)\right. \\
&\times \sinh\alpha(r,t)+\left(2(t_s(r)-t)EE'\sqrt{\frac{3}{2(\Lambda+E^2-8\pi p_0)}}\right. \\
&+ \left.\left. t_0'(r)\sqrt{\frac{(\Lambda+E^2-8\pi p_0)}{6}}\right)\cosh\alpha(r,t)\right]\sinh^{\frac{-1}{2}}\alpha(r,t),
\end{aligned}
\tag{4.2.36}
$$

where

$$
\alpha(r,t)=\sqrt{\frac{2(\Lambda-8\pi p_0+E^2)}{3}}(t_s(r)-t). \tag{4.2.37}
$$

Here, $t_s(r)$ is an arbitrary function of r and is related to the time of formation of the singularity. In the limit $(8\pi p_0 - E^2) \to \Lambda$, the above solution corresponds to the 5D TB solution

$$
\lim_{(8\pi p_0-E^2)\to\Lambda} Y(r,t) = (8M(t_s-t)^2)^{\frac{1}{4}}, \tag{4.2.38}
$$

$$
\lim_{(8\pi p_0-E^2)\to\Lambda} X(r,t) = \frac{M'(t_s-t)+2Mt_s'}{(32M^3(t_s-t)^2)^{\frac{1}{4}}}. \tag{4.2.39}
$$

Case B: Solution with $f(r) \neq 1$

Integrating Eq.(4.2.30) with the conditions $\Lambda-8\pi p_0+E^2>0$ and $f(r)\neq 1$, it follows that

$$
\begin{aligned}
Y(r,t) &= \left[\left(\frac{12M}{\Lambda-8\pi p_0+E^2}-\frac{9(f^2-1)^2}{(\Lambda-8\pi p_0+E^2)^2}\right)^{\frac{1}{2}}\right. \\
&\times \left.\sinh\alpha(r,t)-\frac{3(f^2-1)}{\Lambda-8\pi p_0+E^2}\right]^{\frac{1}{2}}.
\end{aligned}
\tag{4.2.40}
$$

Using Eq.(4.2.40) in (4.2.26), we obtain

$$\begin{aligned}
X(r,t) &= \frac{1}{2f}\left[\left(\frac{12M}{\Lambda-8\pi p_0+E^2}-\frac{9(f^2-1)^2}{(\Lambda-8\pi p_0+E^2)^2}\right)^{\frac{1}{2}}\right. \\
&\times \left.\sinh\alpha(r,t)-\frac{3(f^2-1)}{\Lambda-8\pi p_0+E^2}\right]^{-\frac{1}{2}}\left[\frac{1}{2}\left(\frac{12M}{\Lambda-8\pi p_0+E^2}\right.\right. \\
&- \left.\left.\frac{9(f^2-1)^2}{(\Lambda-8\pi p_0+E^2)^2}\right)^{-\frac{1}{2}}\sinh\alpha(r,t)\left(\frac{12M'}{\Lambda-8\pi p_0+E^2}\right.\right. \\
&- \left.\left.\frac{24MEE'+36ff'(f^2-1)}{(\Lambda-8\pi p_0+E^2)^2}+\left(\frac{36EE'(f^2-1)^2}{(\Lambda-8\pi p_0+E^2)^3}\right)\right)\right. \\
&+ \left.\left(\frac{12M}{\Lambda-8\pi p_0+E^2}-\frac{9(f^2-1)^2}{(\Lambda-8\pi p_0+E^2)^2}\right)^{\frac{1}{2}}\cosh\alpha(r,t)\right. \\
&\times \left.\left(\frac{2EE'}{6(\Lambda-8\pi p_0+E^2)^{\frac{1}{2}}}(t_s(r)-t)+\left(\frac{2(\Lambda-8\pi p_0+E^2)}{3}\right)^{\frac{1}{2}}\right.\right. \\
&\times \left.\left.{t_s}'\right)\left(\frac{6(f^2-1)EE'}{(\Lambda-8\pi p_0+E^2)^2}-\frac{6ff'}{\Lambda-8\pi p_0+E^2}\right)\right],
\end{aligned} \tag{4.2.41}$$

where $\alpha(r,t)$ is given by Eq.(4.2.37). Equations (4.2.40) and (4.2.41) represent the non-marginally bound solution corresponding to $f(r)\neq 1$. One can easily verify the marginally bound solution given by Eqs.(4.2.35) and (4.2.36) by substituting $f(r)=1$ into Eqs.(4.2.40) and (4.2.41). For $E=0$, Eqs.(4.2.35), (4.2.36), (4.2.40) and (4.2.41) reduce to marginally bound and non-marginally bound solutions for 5D perfect fluid collapse case [72].

4.2.3 Apparent Horizons

In this case, apparent horizons can be found by using the boundary of three trapped spheres whose outward normals are null. For the interior metric, this is given as follows

$$g^{\mu\nu}Y_{,\mu}Y_{,\nu}=\dot{Y}^2-(\frac{Y'}{X})^2=0. \tag{4.2.42}$$

Inserting Eqs.(4.2.26) and (4.2.30) in the above equation, we get

$$(\Lambda + E^2 - 8\pi p_0)Y^4 - 6Y^2 + 12M = 0. \tag{4.2.43}$$

In particular, for $\Lambda = 8\pi p_0 - E^2$, we have $Y = \sqrt{2M}$, which is called the Schwarzschild horizon. For $M = 0,\ p_0 = 0$, and $E = 0$, it follows that $Y = \sqrt{\frac{6}{\Lambda}}$, which is called the de-Sitter horizon.

The following positive roots are found from Eq.(4.2.43).

Case (i): For $4M < \frac{3}{\Lambda - 8\pi p_0 + E^2}$, we obtain two horizons

$$Y_{ch} = \sqrt{\frac{3}{\Lambda - 8\pi p_0 + E^2} + \frac{\sqrt{9 - 12M(\Lambda - 8\pi p_0 + E^2)}}{\Lambda - 8\pi p_0 + E^2}}, \tag{4.2.44}$$

$$Y_{bh} = \sqrt{\frac{3}{\Lambda - 8\pi p_0 + E^2} - \frac{\sqrt{9 - 12M(\Lambda - 8\pi p_0 + E^2)}}{\Lambda - 8\pi p_0 + E^2}}. \tag{4.2.45}$$

When $M = 0$, these reduce to $Y_{ch} = \sqrt{\frac{6}{(\Lambda + E^2 - 8\pi p_0)}}$ and $Y_{bh} = 0$.

Case (ii): For $4M = \frac{3}{\sqrt{(\Lambda + E^2 - 8\pi p_0)}}$, we have repeated roots

$$Y_{ch} = Y_{bh} = \frac{3}{\sqrt{(\Lambda + E^2 - 8\pi p_0)}} = Y, \tag{4.2.46}$$

which shows that both horizons coincide. The ranges for the cosmological and the BH horizons are

$$0 \leq Y_{bh} \leq \sqrt{\frac{3}{\Lambda - 8\pi p_0 + E^2}} \leq Y_{ch} \leq \sqrt{\frac{6}{\Lambda - 8\pi p_0 + E^2}}. \tag{4.2.47}$$

The BH horizon has its largest proper area $4\pi Y^2 = \frac{12\pi}{(\Lambda + E^2 - 8\pi p_0)}$, and the cosmological horizon has its area between $\frac{12\pi}{(\Lambda + E^2 - 8\pi p_0)}$ and $\frac{24\pi}{(\Lambda + E^2 - 8\pi p_0)}$.

Case (iii): For $4M > \frac{3}{\sqrt{(\Lambda + E^2 - 8\pi p_0)}}$, there is no positive real root, hence, there is no apparent horizon.

The formation time for the apparent horizon with the help of Eqs.(4.2.35) and (4.2.43) is given by

$$t_N = t_s - \sqrt{\frac{3}{2(\Lambda - 8\pi p_0 + E^2)}}\, \sinh^{-1}\left(\frac{{Y_N}^2}{2M} - 1\right)^{\frac{1}{2}}, \quad (N = 1, 2). \tag{4.2.48}$$

This shows that apparent horizons are formed earlier than singularity, hence the end state of gravitational is BH. In the limit $(8\pi p_0 - E^2) \to \Lambda$, we obtain the result corresponding to 5D TB solution

$$t_{ah} = t_s - \sqrt{\frac{M}{2}}. \tag{4.2.49}$$

Equations (4.2.47) and (4.2.48) imply that $Y_{ch} \geq Y_{bh}$ and $t_{bh} \geq t_{ch}$, respectively. The inequality $t_{bh} \geq t_{ch}$ indicates that the cosmological horizon forms earlier than the BH horizon.

Chapter 5

Phantom Energy Accretion onto 5D Charged Black Hole

Here, we investigate the phantom energy accretion onto 5D charged BH. Babichev et al. [106] have shown that phantom accretion onto the Schwarzschild BH diminishes its mass. Jamil et al. [107] have studied the phantom accretion onto the charged BH. They found that if the BH mass due to accretion of phantom energy becomes smaller than its charge, then it is converted into a NS, which is the violation of CCH. The same conclusion was deduced by Babichev et al. [108], when they studied the phantom energy accretion onto charged BH with generalized linear EoS and Chaplygin gas. In this chapter, we extend the work of Jamil el al. [107] to 5D charged BH. This chapter is organized as follows. In section **5.1**, we formulate the equation of motion for accretion process by using energy conservation, Bernoulli equation and mass flux conservation equation. Section **5.2** is devoted to study the critical accretion. The results of this chapter have been published in the form of a research paper [187].

5.1 Accretion onto 5D Charged Black Hole

In this section, we discuss the phantom energy accretion onto 5D charged BH. We consider a charged static spherically symmetric $N+2$ dimensional BH solution [185]

$$ds^2 = B(r)dt^2 - \frac{1}{B(r)}dr^2 - r^2 d\Omega_N, \tag{5.1.1}$$

where $d\Omega_N$ is the unit N sphere and $B(r) = 1 - \frac{2m}{r^{N-1}} + \frac{Q^2}{r^{2N-2}}$. For $N = 2$, this reduces to 4D conventional RN metric, while for $n = 3$, we get a 5D charged BH solution given by

$$ds^2 = B(r)dt^2 - \frac{1}{B(r)}dr^2 - r^2(d\theta^2 + \sin^2\theta d\phi^2 + \sin^2\theta \sin^2\phi d\psi^2), \tag{5.1.2}$$

where $B(r) = 1 - \frac{2m}{r^2} + \frac{Q^2}{r^4}$. Here m and Q are the mass and charge of BH.

The black hole horizons can be found by solving $B(r) = 1 - \frac{2m}{r^2} + \frac{Q^2}{r^4} \equiv 0$, for r whose positive real roots will give horizons as follows

$$r_1 = \sqrt{m + \sqrt{m^2 - Q^2}}, \quad r_2 = \sqrt{m - \sqrt{m^2 - Q^2}}. \tag{5.1.3}$$

For $m^2 > Q^2$, $r_1 > r_2$, r_1 and r_2 are called outer and inner horizons respectively, for $m^2 = Q^2$, $r_1 = r_2 \equiv m$ (an extremal charged BH) and for $m^2 < Q^2$, both horizons disappear and singularity becomes naked at $r = 0$. For $Q = 0$, $r_1 = 2m$ (Schwarzschild horizon in 4D) and $r_2 = 0$. This implies that like 4D case, the presence of charge is essential for the existence of inner horizon (Cauchy horizon). The regularity of the 5D charged BH can be seen in the regions $r_1 < r < \infty$, $r_2 < r < r_1$ and $0 < r < r_1$.

The energy-momentum tensor for phantom energy is specified by the perfect fluid given by Eq.(2.1.11), in which ρ and p violates the dominant energy condition, i.e., $\rho + p < 0$ and $u^\mu = (u^0, u^1, 0, 0, 0)$ is the five-vector

velocity. We would like to mention here that u^μ satisfies the normalization condition, i.e., $u^\mu u_\mu = 1$. The conservation of the energy-momentum tensor yields

$$r^3 u(\rho + p)\left(B(r) + u^2\right)^{\frac{1}{2}} = A_1, \tag{5.1.4}$$

where A_1 is an integration constant with no dimension and $u^1 = u < 0$ because phantom energy falls radially inward onto BH. By projecting the energy-momentum conservation law on five velocity, we can get energy flux equation, i.e., $u_\mu T^{\mu\nu}{}_{;\nu} = 0$ for which Eq.(2.1.11) leads to

$$r^3 u \exp(s) = -A_2, \tag{5.1.5}$$

where $s = \int_{\rho_\infty}^{\rho_h} \frac{d\hat{\rho}}{\hat{\rho}+p(\hat{\rho})}$, and $A_2 > 0$ is another integration constant which is related to energy flux and has the dimension of r^3. Also, ρ_h and ρ_∞ are phantom energy density at horizon and at infinity. From Eqs.(5.1.4) and (5.1.5), it follows that

$$(\rho + p)\left(B(r) + u^2\right)^{\frac{1}{2}} \exp(-s) = A_3, \tag{5.1.6}$$

where $A_3 = -\frac{A_1}{A_2} = \rho_\infty + p(\rho_\infty)$.

The rate of change of BH mass due to phantom energy accretion is [106]

$$\dot{m} = 2\pi^2 r^3 T^r{}_t.$$

Using Eqs.(5.1.4)-(5.1.6) in the above equation, it follows that

$$\dot{m} = 2\pi^2 A_2(\rho_\infty + p_\infty). \tag{5.1.7}$$

We note that the mass of BH decreases if $(\rho_\infty + p_\infty) < 0$. Thus the accretion of phantom energy onto a BH decreases the mass of BH. As the phantom accretion only diminishes mass and does not affect the charge of BH, so we can deduce that when $m^2 < Q^2$ is reached, then singularity becomes

naked at $r = 0$ and phantom accretion by 5D charged BH may lead to the violation of CCH. This is explained in the next section. It is mentioned here that one can solve Eq.(5.1.7) for m by using EoS $p = \omega\rho$. Since all p and ρ, violating dominant energy condition, must satisfy this equation, hence it holds in general, i.e., $\dot{m} = 2\pi^2 A_2(\rho + p)$.

5.2 Critical Accretion

This section is devoted to analyze the critical points (such points at which flow speed is equal to the speed of sound) during the accretion of phantom energy. The phantom energy falls onto BH with increasing velocity along the particle trajectories. For the discussion of critical accretion points, we follow the procedure of Michel [104]. The conservation of mass flux $J^{\mu}{}_{;\,\mu} = 0$, gives

$$\rho u r^3 = A_4, \tag{5.2.1}$$

where A_4 is another integration constant, which is negative because $u < 0$. From Eqs.(5.1.4) and (5.2.1), it follows that

$$\left(\frac{\rho + p}{\rho}\right)^2 \left(B(r) + u^2\right) = A_5, \tag{5.2.2}$$

where $A_5 = (\frac{A_1}{A_4})^2$. Differentiating Eqs.(5.2.1) and (5.2.2) and ruling out $d\rho$, we get

$$\frac{dr}{r}\left(3V^2 - \frac{2(\frac{m}{r^2} - \frac{Q^2}{r^4})}{B(r) + u^2}\right) + \frac{du}{u}\left(V^2 - \frac{u^2}{B(r) + u^2}\right) = 0, \tag{5.2.3}$$

where $V^2 = \frac{dln(\rho+p)}{dln\rho} - 1$.

The critical points can be found by taking both the factors inside the square brackets equal to zero. Thus, we obtain

$${u_*}^2 = \frac{2}{3}\left(\frac{m{r_*}^2 - Q^2}{r_*^4}\right), \quad {V_*}^2 = \frac{2(m{r_*}^2 - Q^2)}{3{r_*}^4 - 4m{r_*}^2 + Q^2}. \tag{5.2.4}$$

We see that physically acceptable solutions of the above equations are obtained if ${u_*}^2 > 0$ and ${V_*}^2 > 0$ implying that

$$m{r_*}^2 - Q^2 > 0, \quad 3{r_*}^4 - 4m{r_*}^2 + Q^2 > 0. \tag{5.2.5}$$

The subscript $*$ represents a quantity at a point where speed of flow is equal to the speed of sound, such a point is called a critical point.

The fluid particles that move towards a BH initially have flow speed less than speed of sound but as it comes closer to BH horizons, its speed may transit from subsonic to supersonic level. The circular boundary around BH where flow speed is equal to the speed of sound is called a sound horizon. The flow speed is supersonic inside the sound horizons but less than speed of light, as fluid reaches the BH horizon, the flow speed approaches to the speed of light. After crossing the BH horizon, it becomes greater than the speed of light. Notice that the equations corresponding to Eq.(5.2.5) are linear and quadratic in r for 4D charged BH [107].

The positive real roots of the second equation of Eq.(5.2.5) are

$$r_{*_\pm} = \frac{1}{\sqrt{3}}\left(\sqrt{2m \pm \sqrt{4m^2 - 3Q^2}}\right) \tag{5.2.6}$$

which are real if

$$\frac{m^2}{Q^2} \geqslant \frac{3}{4}.$$

These roots represent the position of critical points near a BH. For the solution about critical point, we insert the values of $r_{*\pm}$ from Eq.(5.2.6) in the first equation of Eq.(5.2.5). For r_{*+}, the first equation of Eq.(5.2.5) gives

$$m\sqrt{4m^2 - 3Q^2} \geqslant 3Q^2 - 2m^2, \tag{5.2.7}$$

which is satisfied only if

$$\frac{3}{4} \leqslant \frac{m^2}{Q^2} < \frac{3}{2}. \tag{5.2.8}$$

We would like to mention here that such limits on the mass to charge ratio occur for studying the pseudo-Newtonian force about a charged rotating BH [188].

In phantom energy accretion onto a 4D charged BH, Jamil et al. [106] found such ratio for RN BH as $\frac{8}{9} \leqslant \frac{m^2}{Q^2} < \frac{4}{3}$. It is interesting to note that mass to charge ratio in Eq.(5.2.8) can represent a regular as well extremal 5D RN for lower limit, while upper limit of this ratio can represent a NS. Hence, it is possible that accreting phantom energy onto 5D charged can convert it into NS and CCH can be violated. We would like to mention that increase of dimension does not alter the final fate of charged BH, when phantom energy accretes onto it. Also, for r_{*-}, the first equation of Eq.(5.2.5) gives

$$m\sqrt{4m^2 - 3Q^2} \leqslant 2m^2 - 3Q^2. \tag{5.2.9}$$

For $2m^2 - 3Q^2 < 0$, the above equation yields no solution. We must have $2m^2 - 3Q^2 > 0$ which yields $\frac{m^2}{Q^2} > \frac{3}{2}$. Further, Eq.(5.2.9) is satisfied only for $\frac{m^2}{Q^2} < 1$. Since two ratios are inconsistent in this case, so accretion is not possible through r_{*-}.

Chapter 6

Summary and Discussion

This chapter is devoted to summarize and discuss briefly the results of previous chapters. We also mention some open problems at the end of this chapter.

Gravitational collapse is an open issue in GR, which is highly motivated by CCH. In order to prove or disprove this hypothesis, many efforts have been made by considering different spacetimes and different forms of collapsing matter. To address this issue, we have studied the fate of gravitational collapse in electromagnetic theory by assuming cylindrical and spherical spacetimes. For the spherical gravitational collapse, the collapsing matter has been taken as charged perfect fluid with positive cosmological constant. Also, the scalar fields and polytropic matter have been considered in the charged background. Throughout the thesis, we have used two approaches to discuss the gravitational collapse one by solving the Einstein-Maxwell field equations with perfect fluid and another by using Israel thin shell formalism in charged geometry. We have also studied phantom energy accretion onto 5D charged BH to highlight the status of CCH. The results obtained in thesis can be summarized as follows.

Chapter **TWO** deals with charged perfect fluid cylindrical gravitational

collapse. The analytic solution of the Einstein-Maxwell field equations has been found by assuming that fluid is moving along the geodesics inside the cylindrical symmetry. The method of separation of variables has been used to determine the solution of the field equations. For a particular range of separation constant, the solution represents gravitational collapse. It is found that all physical parameters like density, pressure, electromagnetic field intensity and velocity of the collapsing cylinder become free of initial inhomogeneity. In this case, pressure is a function of time only as in the case of geodesic spherical collapsing model [175]. The essential singularity of solution occurs at a point where the longitudinal length reduces to zero. Since in the limit $r' \to 0$, the Ricci scalar and other physical parameters are finite, so $r' = 0$ is a conical singularity of the metric (2.1.34).

The electromagnetic force associated with electromagnetic field in curved spacetime causes to increase the inhomogeneity of that spacetime. But smoothness in energy density and pressure graphs (Figures **2.2** and **2.3**) represent that electromagnetic field cannot promote inhomogeneity. This is due to the weak electromagnetic field, Figures **2.2** and **2.3** imply that $E < \rho$, which is the condition for a weak electromagnetic field [120]. Using approximate symmetry approach, Hussain et al. [189] have pointed out that presence of fluctuations in energy density indicate gravitational waves. Since fluctuations are absent in energy density graph (Figure **2.2**), so there are no gravitational waves. By matching charged perfect fluid solution with the exterior charged vacuum solution by Darmois junction conditions, we have found:

- Boundary of charged fluid acts as a cylinder of constant proper unit length;

- Coulomb and gravitational forces of system balance each other on boundary of cylinder.

In chapter **THREE**, we have presented thin shell collapse of scalar field and polytropic matter in the charged background. Using the Israel thin shell formalism, we have derived general dynamical equations for thin shell between two RN spacetimes. This general formulation has been applied to scalar field and polytropic matter thin shell explicitly. We have studied the dynamical behavior of scalar field thin shell by treating it as massless and massive. The complete dynamics of scalar field can be described by the equation of motion (3.1.15) and KG equation (3.2.5). These equations cannot be solved exactly, so we have solved them numerically by taking $V(\phi) = \tilde{m}^2\phi^2$ and some initial conditions. This solution is represented in Figure **2.2**, which shows that scalar field shell can expand and collapse. It decays out in the case of expansion, while it inflates to infinity in the case of collapse.

In massless scalar field case, we have found that shell radius is an increasing (decreasing) function of time implying expansion (collapse). Further, $V_{eff}(R)$ in Figures **2.3-2.5** shows that massless scalar field can collapse to a point by forming a curvature singularity or it can expand to infinity. To discuss the massive scalar field case, we have taken p as an explicit function of R and have calculated the scalar potential $V(\phi)$ (3.2.12). In this case, shell radius R behaves like the massless scalar field and $V_{eff}(R) \to -\infty$ as $R \to 0$ (left graph in Figure **2.6**). This shows that shell contracts to zero radius forming a curvature singularity. There is also bouncing behavior of shell in this case as $V_{eff}(R)$ has a well (left graph in Figure **2.6**).

Also, the general formalism has been applied to polytropic matter as

well as perfect fluid thin shell. The dynamics of the system in this case can be described by Eqs.(3.3.3)-(3.3.5). Figure **3.7** describes V_{eff} (3.3.4) for polytropic matter with finite n and initial data of collapsing shell. Also, V_{eff} (3.3.5) for perfect fluid is shown in left graph of Figure **3.8**. These graphs show that $V_{eff} \leqslant 0$, hence Eq.(3.3.3) indicates that motion is possible as $\dot{x}^2 \geqslant 0$. The left graphs in both figures show that V_{eff} varies from $-\infty$ to 0 and from 0 to finite negative value. Since in both these phases motion is always possible, therefore expanding or collapsing matter shell comes to rest and then re-expands or re-collapses. The right graph in Figure **3.7** implies that $V_{eff} \to -\infty$ as $x \to 0$. The matter thin shell expands to infinity or collapses to a point to form a BH or NS. The expanding (collapsing) shell would exhibit bouncing or oscillating behavior, if initial shell velocity is negative (positive).

To study the effects of NC parameter Θ on thin shell gravitational collapse in the charged background, we have adopted the approach introduced by Oh and Park [102]. The geometry part of dynamical equations derived earlier has been left unchanged, while density and pressure of shell have been modified by adding density and pressure of gravitational source due to non-commutativity. The NC version for shell dynamical equations has been derived, which are given by Eqs.(3.3.11)-(3.3.14). The numerical solution of these equations has been presented in Figures **3.9-3.12**. These graphs show that in the presence of NC parameter Θ, an initially expanding or collapsing matter shell comes to rest which cannot re-expand or re-collapse. The solutions for r in $g_{00}(r) = 0$ from Eq.(3.3.6), give the horizons radii. For large value of NC factor Θ, it has been found from Eq.(3.3.13) that the horizon radii cover the singularity at $x_s = 0.00228365$, where density is

singular for the case of polytropic matter with finite n. Thus a regular BH is formed in this case with various horizons. For perfect fluid with infinite n, ρ as well as V_{eff} become singular at $x = 0$. Thus for all values of Θ, the values of horizon radii are greater than zero, hence a singular shell of zero radius seems to be hidden by various concentric circles.

The charged perfect fluid gravitational collapse in Friedmann and 5D TB model with positive constant have been discussed in chapter **FOUR**. In both cases, Darmois junction conditions have been used to find analytic solution of the Einstein-Maxwell field equation and to show the continuity in the gravitational masses of interior and exterior regions. The non-marginally bound solution for 5D TB model and marginally bound solution for Friedmannn as well as 5D have been found. The formation of the apparent horizons and time difference between the formation of apparent horizons and singularity have been discussed for both models. It is found that time of BH horizon formation is larger than cosmological horizon formation, therefore BH is the end state of gravitational collapse. In case of Friedmannm model, Eqs.(4.1.51) and (4.1.52) imply that the time difference between cosmological horizon and singularity is a decreasing function of mass, while time difference between BH horizon and singularity is an increasing function of mass.

To discuss the effects of electromagnetic field and positive cosmological constant on gravitational collapse, we have calculated the rate of gravitational collapse in Friedmann and 5D TB model from Eqs.(4.1.31) and (4.2.30), respectively. The rate of collapse in Friedmann model is

$$(\ddot{a}f_k) = -\frac{M}{(af_k)^2} + (\Lambda + E^2 - 8\pi p_c)\frac{(af_k)}{3}. \tag{6.0.1}$$

This is the acceleration of collapsing matter. For $M \geq \frac{1}{3\sqrt{(\Lambda+E^2-8\pi p_c)}}$ and

$(af_k) \geq \frac{1}{\sqrt{(\Lambda+E^2-8\pi p_c)}}$, we get $\ddot{a}f_k \geq 0$, which implies that there is no collapse of matter at all. For $M < \frac{1}{3\sqrt{(\Lambda+E^2-8\pi p_c)}}$ and $(af_k) < \frac{1}{\sqrt{(\Lambda+E^2-8\pi p_c)}}$, it follows that $(\ddot{a}f_k) < 0$, this is condition for the occurrence of gravitational collapse. Similar analysis can be made from the rate of collapse in 5D TB model, given by the following equation

$$\ddot{Y} = -\frac{2m}{Y^3} + (\Lambda - 8\pi p_c + E^2)\frac{Y}{6}. \tag{6.0.2}$$

We have discussed the phantom energy accretion onto 5D charged BH in chapter **FIVE**. We have derived the equation of motion for phantom energy onto 5D charged BH. It has been found that when phantom energy accretes onto 5D charged BH, then mass of BH goes on decreasing with the passage of time. Since charge of BH remains constant during accretion process, so when amount of charge is larger than the amount of mass, then BH is converted into NS. The critical accretion analysis implies that there exists a unique critical point for which mass to charge ratio is $\frac{3}{4} \leqslant \frac{m^2}{Q^2} < \frac{3}{2}$. This ratio incorporates BHs (extremal and non-extremal for lower bound) and NS (for upper bound). Hence, RN BH in phantom energy dominated universe may provide a process for the formation of NS and CCH can be violated in this case.

In this thesis, we have studied the gravitational collapse of charged perfect collapse and gravitational collapse of thin shell in charged geometry. It would be interesting to investigate the gravitational collapse of charged dissipative fluid in cylindrical and spherical geometries. The thin shell collapse in charged de-Sitter, rotating and charged rotating background would be interesting to explore the status of CCH. The charged perfect fluid cylindrical gravitational collapse can be studied by using symmetry approach introduced by Soh and his collaborators [190, 191] to discuss non-static,

shear-free charged perfect fluid solutions. The 5D TB model collapse can also be extended to some generalized model with $g_{00} \neq 1$. The procedure of phantom energy accretion onto 5D charged BH can be applied to higher dimensional rotating and charged rotating BHs to see the effects of rotation parameter on the accretion process in higher dimension. Several modified theories like $f(R)$ gravity, Gauss-Bonnet gravity and $f(T)$ gravity, are alternative to GR. It would be interesting to extend the work of this thesis in modified theories of gravity.

Bibliography

[1] Hawking, S.W. and Ellis, G.F.R.: *The Large Scale Structure of Space-time* (Cambridge University Press, 1979).

[2] Penrose, R.: Riv. Nuovo Cimento **1**(1969)252.

[3] Joshi, P.S.: *Global Aspects in Gravitation and Cosmology* (Oxford University Press, 1993).

[4] Virbhadra, K.S., Narasimha, D. and Chitre, S.M.: Astron. Astrophys. **337**(1998)1.

[5] Virbhadra, K.S., and Ellis, G.F.R.: Phys. Rev. D **62**(2000)084003.

[6] Virbhadra, K.S., and Ellis, G.F.R.: Phys. Rev. D **65**(2002)103004.

[7] Paschoff, J.M.: *Contemporary Astronomy* (Harcourt Brace College Publishers, 1981).

[8] Claudel, C.M., Virbhadra, K.S. and Ellis, G.F.R.: J. Math. Phys. **42**(2001)818.

[9] Virbhadra, K.S. and Keeton, C.R.: Phys. Rev. D **77**(2008)124014.

[10] Virbhadra, K.S.: Phys. Rev. D **60**(1999)104041.

[11] Seifert, H.: Proc. American Math. Soc. **1**(1950)287.

[12] Virbhadra, K.S.: Phys. Rev. D **79**(2009)083004.

[13] Oppenheimer, J.R. and Snyder, H.: Phys. Rev. **56**(1939)455.

[14] Lemaitre, G.: Ann. Soc. Sci. Bruxelles A **53**(1933)51.

[15] Tolman, R.C.: Proc. Nat. Acad. Sci. **20**(1934)169.

[16] Bondi, H.: Mon. Not. Roy. Astron. Soc. **107**(1947)410.

[17] Singh, T.P. and Witten, L.: Class. Quantum Grav. **14**(1997)3489.

[18] Herrera, L., Di Prisco, A., Hernandez-Pastora, J.L. and Santos, N.O.: Phys. Lett. A **237**(1998)113.

[19] Joshi, P.S.: *Singularities, Black Holes and Cosmic Censorship* (IUCAA Publishing, 1997).

[20] Misner, C.W. and Sharp, D.: Phys. Rev. **136**(1964)b571.

[21] Vaidya, P.C.: Proc. Indian Acad. Sci. A **33**(1951)264.

[22] Santos, N.O.: Phys. Lett. A **106**(1984)296.

[23] Ori, A. and Piran, T.: Phys. Rev. Lett. **59**(1987)2137.

[24] Ori, A. and Piran, T.: Gen. Relativ. Gravit. **20**(1988)7.

[25] Ori, A. and Piran, T.: Phys. Rev. D **42**(1990)1068.

[26] Joshi, P.S. and Dwivedi, I. H.: Commun. Math. Phys. **146**(1992)333.

[27] Hinshaw, G. et al. Astrophys. J. Suppl. **180**(2009)225.

[28] Markovic, D. and Shapiro, S.L.: Phys. Rev. D **61**(2000)084029.

[29] Khan, I. and Qadir, A.: *Proc. Fourth Marcel Grossmann Meeting*, ed. Ruffini, R. (Elsevier Science Publishers, 1986).

[30] Lake, K.: Phys. Rev. D **62**(2000)027301.

[31] Ghosh, S.G. and Deshkar, D.W.: Astrophys. Space Sci. **310**(2007)111.

[32] Sharif, M. and Ahmad, Z.: Mod. Phys. Lett. A **22**(2007)1493; *ibid.* 2947.

[33] Debnath, U., Nath, S. and Chakraborty, S.: Gen. Relativ. Gravit. **37**(2005)215.

[34] Abramovici, A. et al.: Science **256**(1992)325.

[35] Caron, B. et al. Class. Quantum Grav. **14**(1997)1461.

[36] L*ü*ck, H. and the GEO600 Team: Class. Quantum Grav. **14**(1997)1471.

[37] Piran, T.: Phys. Rev. Lett. **41**(1978)1085.

[38] Echeverria, F.: Phys. Rev. D **47**(1993)2271.

[39] Chiba, T.: Prog. Theor. Phys. **95**(1996)321.

[40] Nakao, K. and Morisawa, Y.: Class. Quantum Grav. **21**(2004)2101.

[41] Nakao, K. and Morisawa, Y.: Phys. Rev. D **71**(2005)124007.

[42] Kurita, Y. and Nakao, K.: Phys. Rev. D **73**(2006)064002.

[43] Bronnikov, K.A. and Kovalchuk, K.A.: *Problemy Teorii Gravitatsii i Elementarnykh Chastits* **11**(1980)131 (in Russian).

[44] Bronnikov, K.A. and Kovalchuk, K.A.: Gen. Relativ. Gravit. **15**(1983)809.

[45] Bronnikov, K.A. and Kovalchuk, K.A.: Gen. Relativ. Gravit. **15**(1983)823.

[46] Hayward, S.A.: Class. Quantum Grav. **17**(2000)1749.

[47] Oron, A.: Phys. Rev. D **66**(2002)023006.

[48] Nolan, B.C.: Phys. Rev. D **65**(2002)104006.

[49] Nakao, K. and Morisawa, Y.: Prog. Theor. Phys. **113**(2005)73.

[50] Sharif, M. and Ahmad, Z.: Gen. Relativ. Gravit. **39**(2007)1331.

[51] Di Prisco, A., Herrera, L., MacCallum, M.A.H. and Santos, N.O.: Phys. Rev. D **80**(2009)064031.

[52] Israel, W.: Nuovo Cimento B **44**(1966)1.

[53] Israel, W.: Nuovo Cimento B **48**(1967)463(**E**).

[54] De La Cruz, V. and Israel, W.: Nuovo Cimento A **51**(1967)744.

[55] Kuchar, K.: Czechoslovak J. Phys. B **18**(1968)435.

[56] Chase, J.E.: Nuovo Cimento B **67**(1970)136.

[57] Boulware, D.G.: Phys. Rev. D **8**(1973)2363.

[58] Kijowski, J. and Magli, G.: Int. J. Mod. Phys. D **18**(2009)1801.

[59] Pereira, P.R.C.T. and Wang, A.: Phys. Rev. D **62**(2000)124001; *ibid.* D **67**(2003)129902.

[60] Sharif, M. and Ahmad, Z.: Int. J. Mod. Phys. A **23**(2008)181.

[61] Sharif, M. and Iqbal, K.: Mod. Phys. Lett. A **24**(2009)1533.

[62] Sharif, M. and Abbas, G.: Gen. Relativ. Gravit. **43**(2011)1179.

[63] Kaluza, T.: Sitz. Preuss. Akad. Wiss. Phys. Math. **K1**(1921)966. (Eng. Trans. in [64, 65])

[64] *Unified Field Theories of More Than 4 Dimensions, Proc. International School of Cosmology and Gravitation*, eds. De Sabbata, V. and Schmutzer, E. (World Scientific, 1983).

[65] *An Introduction to Kaluza-Klein Theories, Proc. Chalk River Workshop on Kaluza-Klein Theories*, ed. Lee, H.C. (World Scientific, 1984).

[66] Klein, O.: Zeits. Phys. **37**(1926)895. (Eng. Trans. in [64, 65])

[67] Schwarz, J.J.: Nucl. Phys. B **226**(1983)269.

[68] Ilha, A. and Lemos, J.P.S.: Phys. Rev. B **55**(1997)1788.

[69] Sil, A. and Chatterjee, S.: Gen. Relativ. Gravit. **26**(1994)999.

[70] Ghosh, S.G. and Saraykar, S.: Phys. Rev. D **62**(2000)107502.

[71] Ghosh, S.G., Deshkar, D.W. and Saste, N.N: Int. J. Mod. Phys. D **16**(2007)53.

[72] Sharif, M. and Ahmad, Z.: J. Korean Phys. Soc. **52**(2008)980.

[73] Sharif, M. and Ahmad, Z.: Acta Phys. Polonica B **39**(2008)1337.

[74] Jhingan, S. and Ghosh, S.G.: Phys. Rev. D **81**(2010)024010.

[75] Maeda, H.: Phys. Rev. D **73**(2006)104004.

[76] Banerjee, A., Debnath, U. and Chakraborty, S.: Int. J. Mod. Phys. D **12**(20003)1255.

[77] Wheeler, J.A.: Phys. Rev. **97**(1955)511.

[78] Brill, D.R. and Wheeler, J.A.: Phys. Rev. **105**(1957)1662.

[79] Jacobson, T.: Phys. Rev. Lett. **83**(1999)2699.

[80] Kaup, D.J.: Phys. Rev. **172**(1968)1331.

[81] Ruffini, R. and Bonazzola, S.: Phys. Rev. **187**(1969)1767.

[82] Christodoulou, D.: Ann. Math. **140**(1994)607.

[83] Choptuik, M.W.: Phys. Rev. Lett. **70**(1993)9.

[84] Evans, C.R. and Coleman, J.S.: Phys. Rev. Lett. **72**(1994)1782.

[85] Roberts, M.D.: Gen. Relativ. Gravit. **21**(1989)907.

[86] Bardy, P.R.: Class. Quantum Grav. **11**(1996)1255.

[87] Malec, E.: Class. Quantum Grav. **13**(1995)1849.

[88] Gundlach, C.: Phys. Rev. Lett. **75**(1995)3214.

[89] Goncalves, S.M.C.V.: Phys. Rev. D **62**(2000)124006.

[90] Chambers, C.M., Brady, P.R. and Goncalves, S.M.C.V.: *Proc. Eighth Marcel Grossmann Meeting on General Relativity*, ed. Piran, T. (World Scientific, 1997).

[91] Virbhadra, K.S., Jhingan, S. and Joshi, P.S.: Int. J. Mod. Phys. D **6**(1997)357.

[92] Goswami, R. and Joshi, P.S.: Phys. Rev. D **76**(2007)084026.

[93] Bhattacharya, S., Goswami, R. and Joshi, P.S.: Int. J. Mod. Phys. D **20**(2011)1123.

[94] Núñez, D., Quevedo, H. and Salgado, M.: Phys. Rev. D **58**(1998)083506.

[95] Mann, R.B. and Nicoloni, P.: Phys. Rev. D **84**(2011)064014.

[96] Nicoloni, P., Smailagic, A., and Spallucci, E.: Phys. Lett. B **632**(2006)547.

[97] Ansoldi, S., Nicoloni, P., Smailagic, A., and Spallucci, E.: Phys. Lett. B **645**(2007)261.

[98] Modesto, L. and Nicolini, P.: Phys. Rev. D **82**(2010)104035.

[99] Bastos, C., Bertolami, O., Dias, N.C. and Prata, J.N.: Phys. Rev. D **80**(2009)124038.

[100] Bastos, C., Bertolami, O., Dias, N.C. and Prata, J.N.: Phys. Rev. D **84**(2011)024005.

[101] Bertolami, O. and Zaro, C.D.A.: Phys. Rev. D **81**(2010)025005.

[102] Oh, J.J. and Park, C.: J. High Energy Phys. **03**(2010)86.

[103] Bondi, H.: Mon. Not. Roy. Astron. Soc. **112**(1952)195.

[104] Michel, F.C.: Astrophys. Space Sci. **15**(1972)153.

[105] Sun, C.Y.: Phys. Rev. D **78**(2008)064060.

[106] Babichev, E., Dokuchaev, V. and Eroshenko, Y.: Phys. Rev. Lett. **93**(2004)021102.

[107] Jamil, M., Rashid, M. and Qadir, A.: Eur. Phys. J. C **58**(2008)325.

[108] Babichev, E., Dokuchaev, V. and Eroshenko, Y.: J. Exp. Theor. Phys. **112**(2011)784.

[109] Madrid, J.A.J. and Gonzalez, P.F.: Gravitation and Cosmology **14**(2008)213.

[110] Sharif, M. and Abbas, G.: Chin. Phys. Lett. **28**(2011)090402.

[111] Sharif, M. and Abbas, G.: Chin. Phys. Lett. **29**(2012)010401.

[112] Sharif, M. and Abbas, G.: J. Phys.: Conf. Ser. **354**(2012)012019.

[113] Thorne, K.S.: Phys. Rev. **138**(1965)B251.

[114] Thorne, K.S.: Phys. Rev. **139**(1965)B244.

[115] Ardavan, H. and Partovi, M.H.: Phys. Rev. D **16**(1977)1664.

[116] Stein-Schabes, J.A.: Phys. Rev. D **31**(1985)1838.

[117] Germani, C. and Tsagas, C.G.: Phys. Rev. D **73**(2006)064010.

[118] Kouretsis, A.P. and Tsagas, C.G.: Phys. Rev. D **82**(2010)124053.

[119] Tsagas, C.G.: Phys. Rev. D **72**(2005)123509.

[120] Tsagas, C.G.: Class. Quantum Grav. **22**(2005)393.

[121] Barrow, J.D. and Tsagas, C.G.: Class. Quantum Grav. **26**(2006)195003.

[122] Tsagas, C.G.: Phys. Rev. D**75**(2007)087901.

[123] Barrow, J.D. and Tsagas, C.G.: Phys. Rev. D **77**(2008)107302.

[124] Spyrou, N.K. and Tsagas, C.G.: Mon. Not. Roy. Astron. Soc. **388**(2008)187.

[125] Tsagas, C.G.: Phys. Rev. Plasma Phys. Control Fusion **51**(2009)124013.

[126] Tsagas, C.G.: Phys. Rev. D **81**(2010)043501.

[127] Tsagas, C.G.: Mon. Not. Roy. Astron. Soc. **405**(2010)503.

[128] Tsagas, C.G.: Phys. Rev. D **84**(2011)043524.

[129] Tsagas, C.G.: Phys. Rev. D **84**(2011)063503.

[130] Barrow, J.D. and Tsagas, C.G.: Mon. Not. Roy. Astron. Soc. **414**(2011)512.

[131] Herrera, L., Di Prisco, A. and Ibanez, J.: Phys. Rev. D **84**(2011)107501.

[132] Di Prisco, A., Herrera, L., Denmat, G.Le., MacCallum, M.A.H. and Santos, N.O.: Phys. Rev. D **76**(2007)064017.

[133] Sharif, M. and Bhatti, M.Z.: Gen. Relativ. Gravit. DOI 10.1007/s10714-012-1428-2.

[134] Sharif, M. and Bhatti, M.Z.: Mod. Phys. Lett. A **27**(2012)1250141.

[135] Eddington, A.S.: *Internal Constitution of the Stars* (Cambridge University Press, 1926).

[136] Rosseland, S.: Mon. Not. Roy. Astron. Soc. **84**(1924)720.

[137] Bally, J. and Harrison, E.R.: Astrophys. J. **220**(1978)743.

[138] Ray, S., Malheiro, M., Lemos, J.P.S. and Zanchin, V.T.: Braz. J. Phys. **34**(2004)310.

[139] Landau, L.D. and Lifshitz, E.M.: *The Classical Theory of Fields* (Addison-Willy Press, 1962).

[140] Stephani, H.: *General Relativity* (Cambridge University Press, 1990).

[141] Jackson, J.D.: *Classical Electrodynamics* (John Wiley and Sons, 1999).

[142] Pant, N., Tewari, B.C. and Fuloria, P.: J. Mod. Phys. **02**(2011)1538.

[143] Graves, J.C. and Brill, D.R.: Phys. Rev. **120**(1960)1507.

[144] Bonnor, W.B.: Mon. Not. Roy. Astron. Soc. **137**(1965)239.

[145] Singh, T.P.: J. Astrophys. Astron. **20**(1999)221.

[146] Harada, T., Iguchi, H. and Nakao, K.: Prog. Theor. Phys. **107**(2002)449.

[147] Joshi, P.S. and Malafarina, D.: Int. J. Mod. Phys. D **20**(2011)2641.

[148] Frauendiener, J. and Klien, C.: J. Math. Phys. **36**(1995)3632.

[149] Joshi, P.S.: *Gravitational Collapse and Spacetime Singularities* (Cambridge University Press, 2007).

[150] Plenbanski, J. and Krasinki, A.: *An Introduction to General Relativity and Cosmology* (Cambridge University Press, 2006).

[151] Nolan, B.C.: Phys. Rev. D **60**(1999)024014.

[152] Nakao, K., Harada, T. and Miyamoto, U.: Phys. Rev. D **82**(2010)121501.

[153] Królak, A.: J. Math. Phys. **28**(1987)138.

[154] Wheeler, J.A.: *Magic Without Magic: John Archibald Wheeler, A Collection of Essays in Honor of His 60th Birthday* ed. Klauder, J.R. (Freeman Press, 1972).

[155] Hobson, M.P., Efstathiou, G. and Lasenby, A.N.: *General Relativity: An Introduction for Physicists* (Cambridge University Press, 2006).

[156] Penrose, R.: Phys. Rev. Lett. **14**(1965)57.

[157] Malec, E. and Murchadha, N.O.: Phys. Rev. D **47**(1993)1454.

[158] Hawking, S.W.: Commun. Math. Phys. **25**(1972)152.

[159] Thornburg, J.: Living Rev. Relativ. **10**(2007)03.

[160] Gyulchev, G.N. and Yazadjiev, S.S.: Phys. Rev. D **75**(2007)23006.

[161] Soldner, J.: Berliner Astron. Jahrb. **1804**(1801)161.

[162] Einstein, A.: Annalen der Physik **35**(1911)898.

[163] Schutz, B.: *Gravity from the ground up* (Cambridge Unversity Press, 1993).

[164] Perlmutter, S. et al.: Nature **391**(1998)51.

[165] Perlmutter, S. et al.: Astrophys. J. **517**(1999)565.

[166] Brasselet, J.P.: *Proc. NATO Advanced Study Institute on New Developments in Singularity Theory*, eds. Siersma, D., Wall, C.T.C. and Zakalyukin, V. (Kluwer Academic Publishers, 2000).

[167] Khalil, S. and Munoz, C.: Contemp. Phys. **43**(2002)51.

[168] Jetzer, P.: Phys. Rep. **220**(1992)163.

[169] Mielke, E.W. and Schunck, F.E.: Nucl. Phys. B **564**(2000)185.

[170] Dandach, N.F.: IL Nuovo Cimento B **107**(1992)1267.

[171] Lanczós, C.: Phys. Z. **23**(1922)539.

[172] Lanczós, C.: Ann. Phys. **74**(1924)518.

[173] Darmois, G. *Les équations de la Gravitation einsteinienne. Mèmorial des sciences Mathématique, part XXV* (Gauthier-Villars, Paris, 1927).

[174] Brien, O.S. and Synge, J.L.: *Jump Conditions at Discontinuities in General Relativity*(Institute for Advanced Studies, 1952).

[175] Brandt, C.F.C., Chan, R., da Sliva, M.F.A. and da Rocha, J.F.V.: Int. J. Mod. Phys. D **19**(2010)317.

[176] Sharif, M. and Abbas, G.: J. Phys. Soc. Jpn. **80**(2011)104002.

[177] Di Prisco, A., Herrera, L., MacCallum, M.A.H. and Santos, N.O.: Phys. Rev. D **80**(2009)64031.

[178] Chao-Guang, H.: Acta Physica Sinica **4**(1995)617.

[179] Sharif, M. and Abbas, G.: Gen. Relativ. Gravit. **44**(2012)2353.

[180] Sharif, M. and Abbas, G.: J. Phys. Soc. Jpn. **81**(2012)044002.

[181] Mann, R.B. and Oh, J.J.: Phys. Rev. D **74**(2006)124016.

[182] Mann, R.B., Oh, J.J. and Mu-In, P.: Phys. Rev. D **79**(2009)64005.

[183] Sharif, M. and Abbas, G.: Astrophys. Space Sci. **327**(2010)285

[184] Sharif, M. and Abbas, G.: J. Korean Phys. Soc. **56**(2010)529.

[185] Bakshi, A.V. and Bakshi, U.A.: *Field Theory* (Technical Publishing, 2007).

[186] Konoplya, R.A. and Zhidenko, A.: Phys. Rev. Lett. **103**(2009)161101.

[187] Sharif, M. and Abbas, G.: Mod. Phys. Lett. A **26**(2011)1731.

[188] Qadir, A.: Eur. Phys. Lett. **2**(1986)427.

[189] Hussain, I., Mahomed, F.M. and Qadir, A.: Phys. Rev. **D79**(2009)125014.

[190] Soh, C.W. and Mahomed, F.M.: Class. Quantum Grav. **17**(2000)3063.

[191] Mahomed, F.M., Qadir, A. and Soh, C.W.: Nuovo Cimento B **118**(2003)373.

Appendix

List of Publications

This thesis has resulted the following papers which have been published and attached herewith.

1. Sharif, M. and **Abbas, G.**: *Charged Perfect Fluid Cylindrical Gravitational Collapse*, J. Phys. Soc. Jpn. **80**(2011)104002.

2. Sharif, M. and **Abbas, G.**: *Expanding and Collapsing Scalar Field Thin Shell*, Gen. Relativ. Gravit. **44**(2012)2353.

3. Sharif, M. and **Abbas, G.**: *Non-Commutative Correction to Thin Shell Collapse in Reissner-Nordström Geometry*, J. Phys. Soc. Jpn. **81**(2012)044002.

4. Sharif, M. and **Abbas, G.**: *Gravitational Charged Perfect Fluid Collapse in Friedmann Universe Models*, Astrophys. Space Sci. **327**(2010)285.

5. Sharif, M. and **Abbas, G.**: *Effects of the Electromagnetic Field on Five Dimensional Gravitational Collapse*, J. Korean Phys. Soc. **56**(2010)529.

6. Sharif, M. and **Abbas, G.**: *Phantom Accretion by Five Dimensional Charged Black Hole*, Mod. Phys. Lett. A **26**(2011)1731.

Also, the following papers related to this thesis have been published/submitted.

1. Sharif, M. and **Abbas, G**.: *Gravitational Collapse: Expanding and Collapsing Regions*, Gen. Relativ. Gravit. **43**(2011)1179.

2. Sharif, M. and **Abbas, G.**: *Dynamics of Non-adiabatic Charged Cylindrical Gravitational Collapse*, Astrophys. Space Sci. **335**(2011)515.

3. Sharif, M. and **Abbas, G.**: *Phantom Accretion onto the Schwarzschild de-Sitter Black Hole*, Chin. Phys. Lett. **28**(2011)090402.

4. Sharif, M. and **Abbas, G.**: *Phantom Accretion by Stringy Charged Black Hole*, Chin. Phys. Lett. **29**(2012)010401.

5. Sharif, M. and **Abbas, G.**: *Phantom Energy Accretion by a Class of Black Holes*, J. Phys.: Conf. Ser. **354**(2012)012019.

6. Sharif, M. and **Abbas, G.**: *Dynamics of Shearfree Dissipative Collapse in $f(G)$ Gravity*, (Submitted for Publication).

7. Sharif, M. and **Abbas, G.**: *Singularities of Noncompact Charged Objects*, (Submitted for Publication).

8. Sharif, M. and **Abbas, G.**: *Perfect Fluid Accretion by the Interior of Black Hole*, (Submitted for Publication).